Journal of Geovisualization and Spatial Analysis (2026) 10:27
https://doi.org/10.1007/s41651-026-00269-0

RESEARCH

PERMACLIM 2.0: a Revised Model for High-Resolution Mapping of Permafrost Conditions in Mountain Regions

Edoardo Riva[1,2] · Stefano Ponti[2,3] · Mauro Guglielmin[2,3]

Received: 7 February 2026 / Accepted: 27 May 2026

Abstract

In the current climate change scenario, it is increasingly important to evaluate mountain areas potentially at risk in an efficient and rapid way. Permafrost is one of the main factors determining surface stability in mountain regions. The monitoring network of ground surface thermistors is limited and in several cases the data and metadata are not of easy access. Therefore, modelling is a valid alternative for the prediction of the ground surface temperature (GST). This work presents an update version of the physics-based model PERMACLIM (PERMACLIM 2.0) for the calculation of the mean annual ground surface temperature (MAGST) and for mapping permafrost conditions. PERMACLIM 2.0 presents several updates mainly regarding the realization of the snow depth maps, the calculation of the GST and the classification of the MAGST for detecting permafrost conditions in terms of presence, probability, possibility and absence of permafrost aggradation. The model was tested for the hydrological years 2020 and 2022, on the entire upper Valtellina, in the Northern Central Italian Alps, returning results with a spatial resolution of 10 m. The overall RMSE for MAGST ranges between 0.6 and 0.8 °C. The permafrost conditions were not favourable for the 67.8%, slightly favourable for the 8%, favourable for the 17.9% and very favourable for the 6.2%. The good results obtained and the new design of the model suggest using PERMACLIM 2.0 as a new tool to determine permafrost conditions useful to update the vulnerability and the risk maps in mountain regions.

Keywords Mountain permafrost · Alps · Permafrost modelling · GST

Introduction

The increase in temperature is not uniform across the planet. The environments most sensitive and vulnerable to climate warming are boreal regimes (Cohen et al. 2014), Arctic regions (Serreze and Barry 2011), and mountain areas (Pepin et al. 2022). In particular, the European Alps experienced an air temperature increase of 0.45 °C per decade between 1993 and 2022 (Noetzli et al. 2025). The effects of climate change in the Alps are evident in both biotic and abiotic environments (Cannone et al. 2007, 2008; Guglielmin et al. 2021). Abiotic consequences have been highlighted primarily regarding glacier shrinkage, debris cover, and permafrost degradation (Haeberli and Beniston 1998; Harris et al. 2003; Colucci and Guglielmin 2015).

Glacial retreat and permafrost degradation increase the vulnerability of mountain regions, prompting scientists to monitor and assess risks to humans and infrastructure (e.g., Duvillard et al. 2021) to mitigate adverse effects. The response of permafrost to climate change is more complex than that of glaciers, as direct observations are not always feasible.

Permafrost monitoring remains limited in terms of both temporal series and spatial coverage. Only a few boreholes capture Essential Climate Variables (ECVs) in mountain environments. The PACE (Permafrost and Climate in Europe) project initiated a more systematic and standardized monitoring approach in 1998 (Harris et al. 2003). Since

✉ Mauro Guglielmin
mauro.guglielmin@uninsubria.it

Edoardo Riva
eriva5@uninsubria.it

Stefano Ponti
stefano.ponti@uninsubria.it

[1] Via Valleggio 11, University of Insubria, Como, Italy

[2] Via Dunant 3, Climate Change Research Center, Varese, Italy

[3] Via Dunant 3, University of Insubria, Varese, Italy

Published online: 10 June 2026

then, several studies (e.g., Guglielmin et al. 2018; Etzelmüller et al. 2020) have described the evolution of permafrost in Europe and the Alps, emphasizing rapid warming and degradation over the last 25 years. The mean permafrost warming rate for the European Alps, calculated with the latest data at 10 m depth, is 0.36 °C per decade (Noetzli et al. 2025). However, boreholes are expensive and provide only point-specific descriptions of permafrost status.

Therefore, models represent a suitable alternative for studying permafrost over large areas. Widely used approaches include: Semi-empirical models, such as PERMAKART (Keller 1992), PERMAMAP (Hoelzle 1992), and APMOD (Boeckli et al. 2012a), the latter of which informs the Alpine Permafrost Index Map (APIM, Boeckli et al. 2012b); Remote sensing-based models (Ou et al. 2016); Physical models, such as TTOP (Henry and Smith 2001), PERMEBAL (Stocker-Mittaz et al. 2002), or various versions of CryoGRID (Gisnås et al. 2013; Westermann et al. 2013, 2016, 2023). Guglielmin et al. (2003) developed PERMACLIM, a physics-based model for mapping permafrost distribution in mountain catchments using Mean Annual Ground Surface Temperature (MAGST) as a proxy for permafrost presence.

PERMACLIM was designed to operate using readily available data from Automatic Weather Stations (AWS) in the Italian Alps, such as air temperature (Ta) and snow depth (HS). The model also requires a Digital Elevation Model (DEM) to calculate topographic features. The simplicity and versatility of PERMACLIM led the Piemonte Regional Environmental Protection Agency (ARPA Piemonte) to adopt it for permafrost monitoring and the development of an initial QGIS tool. Although the APIM provides probabilistic estimates at a 25 m resolution, rapid warming necessitates a tool capable of quickly assessing current permafrost conditions using recent data to allow authorities to monitor vulnerable areas effectively.

The aim of this work is to present PERMACLIM 2.0, a model for determining permafrost conditions on a large scale with a spatial resolution of 10 m through a simple and replicable GIS procedure. To achieve this, we model the ground surface temperature over the minimum period required for permafrost formation (two consecutive years, Muller 1945), rather than the longer periods used in the original version. PERMACLIM 2.0 updates the previous tool with significant improvements to factors influencing the surface energy balance (e.g., snow, radiation). Consequently, the model can be used to identify potential degradation (or aggradation) and map permafrost vulnerability to assess hazards rapidly and efficiently.

Unlike the previous release, PERMACLIM 2.0 utilizes data from AWS located within the same pluviometric region. The update includes several enhancements, primarily concerning snow modelling, as snow is a dominant factor affecting Ground Surface Temperature (GST) due to its insulating effect (French 2017). These updates include: (a) improved temporal resolution to capture rapid snow changes during autumn and spring; (b) calculation of snow density and thermal conductivity; (c) updated empirical factors for simulating avalanche phenomena and wind transport; (d) the introduction of a snowmelt factor.

GST calculation during the snow-free summer period has also been refined with a radiative correction factor. Moreover, for more realistic sub-snow GST calculations, sensible heat fluxes (Qs) were computed using all available data from the Italian territory.

This article also demonstrates how these improvements enhance the model's predictive power through a user-friendly procedure. The results improve the modelling of snowpack distribution during the melting period and quantify the impact of these improvements on GST calculations.

Finally, PERMACLIM 2.0 introduces a new classification system, based on theoretical literature, to determine permafrost conditions. MAGST maps were reclassified to identify where permafrost conditions are very favorable, favorable, slightly favorable, or absent.

Study Area

PERMACLIM 2.0 was tested in a region of the Central Italian Alps where extensive data are available for validation. This area previously served as the testing ground for the original PERMACLIM (Guglielmin et al. 2003) and concentrates the majority of permafrost temperature records for the Italian Alps, including the longest available time series (Guglielmin et al. 2001, 2018; Guglielmin 2004; Etzelmüller et al. 2020; Noetzli et al. 2025). Furthermore, numerous studies on ice content (Guglielmin et al. 2004; Stenni et al. 2007), active layer monitoring (Ponti et al. 2024), and periglacial landforms (Cannone and Gerdol 2003; Guglielmin et al. 2021, 2022) have been conducted here. The study area covers 1645.8 km² and encompasses the Upper Valtellina and the neighboring Trentino-Alto Adige territory.

Given the high spatial variability of climatic parameters in Alpine environments (Gobiet et al. 2014), particularly for winter precipitation (Bartolini et al. 2009), the boundaries of the study area were defined based on the precipitation map proposed by Pavan et al. (2019). Additionally, a minimum elevation threshold of 2000 m a.s.l. was established, as the lower permafrost limit for this sector of the Alps is approximately 2500 m a.s.l. (Oliva et al. 2018) (Fig. 1). The region is characterized by a continental Alpine climate (Soncini et al. 2016). A 40-year meteorological analysis (1978–2018)

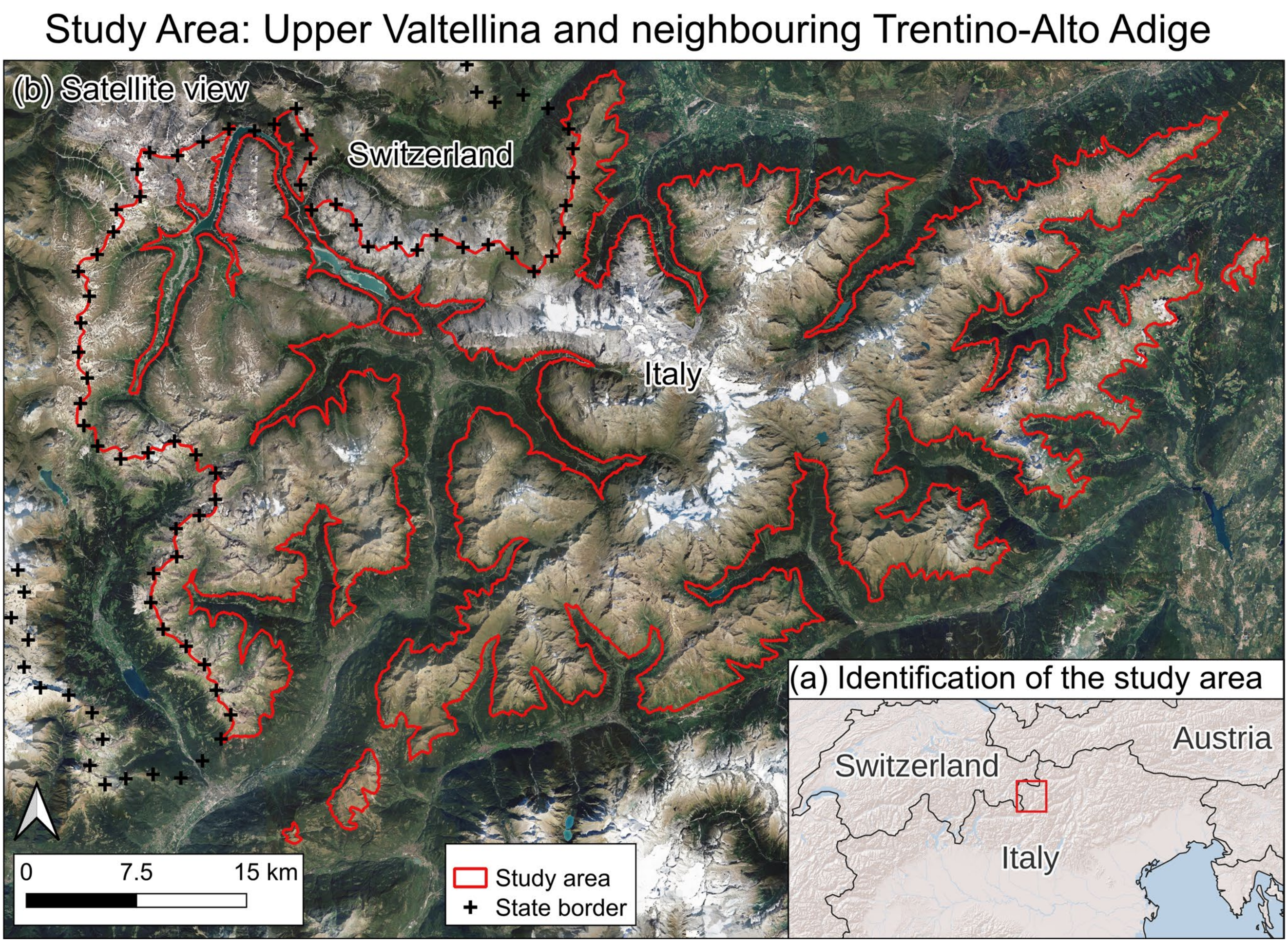

Fig. 1 **(a)** Identification of the study area (red rectangle) in northern Italy (Sources: ESRI Shaded Relief and QGIS World map). **(b)** Satellite view (Source: Google Maps) of the study area (red perimeter) including the Italian state border (Source: Instituto Nazionale di Statistica)

from the station near the Cancano Lakes (46° 31′ 02.2″N, 10° 19′ 14.7″E, 1948 m a.s.l.) shows a mean annual air temperature of + 3.3 ± 0.8 °C and a mean annual cumulative precipitation of 817 mm (Malfasi and Cannone 2021).

In detail, permafrost distribution in the Stelvio Pass area is sporadic between 2400 and 2700 m a.s.l. (Cannone et al. 2003a, b) and becomes discontinuous above that elevation (Guglielmin and Siletto 2000). Nevertheless, data from the PACE borehole, drilled near the Pass at 3000 m a.s.l., indicates that permafrost thickness exceeds 200 m (Guglielmin et al. 2018).

Input Data

Mean daily air temperature (Ta, °C) and snow depth (HS, cm) were collected from 11 AWS (8 for the training set and 3 for the validation of temperature and snow depth maps) located within the study area above 1500 m a.s.l. (Fig. 2). The stations were selected along an altitudinal transect to capture the full spatial variability of the measurements. Data were kindly provided by the Lombardia Regional Environmental Protection Agency (ARPA Lombardia, https://www.arpalombardia.it), the Autonomous Province of Bolzano (https://meteo.provincia.bz.it), the Autonomous Province of Trento (https://www.meteotrentino.it), and the A2A group, in addition to the research group's Stelvio ITEX weather station.

A time interval of two hydrological years, from 01/10/2020 to 30/09/2022, was considered to cover the minimum time frame required to define permafrost conditions (French 2017). The digital elevation model (DEM) used was the TIN ITALY version 1.1 (Tarquini et al. 2023), produced by the National Institute of Geophysics and Volcanology (INGV) with a spatial resolution of 10 m. The choice of this 10 m spatial grid represents a compromise between the distribution patterns of ground surface temperature (GST) in such a heterogeneous and rugged environment and the representativeness of the available climatic data.

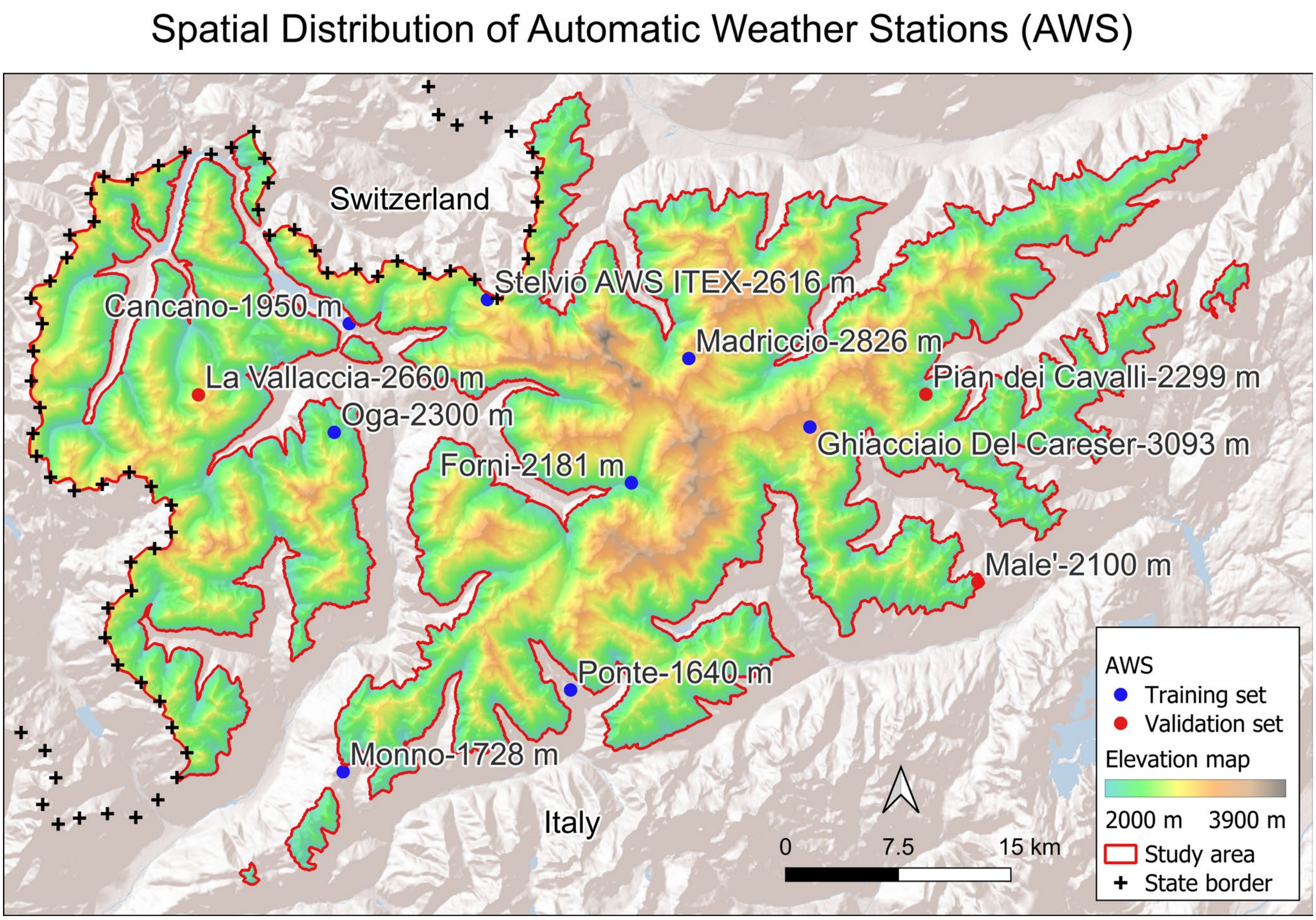

Fig. 2 Study area and AWS. As elevation map was used the TIN Italy version 1.1 (Tarquini et al. 2023). The base map comes from the ESRI Shade Relief

PERMACLIM 2.0

Updates to the Spatialization of the Input Data

Our objective is to model climate variables at a weekly or monthly resolution using the simplest and most replicable approach possible. This is feasible because phenomena such as temperature inversions or local circulation patterns, which occur on limited timescales, were not detectable at this resolution. Consequently, linear regression was considered the most effective method for modelling air temperature.

A similar approach was adopted for generating snow depth maps. Since both air temperature and snow depth are strongly dependent on altitude (Rolland 2003; Beniston 2006; Grünewald et al. 2014), the maps were created by deriving linear regression coefficients between elevation and the mean values of these two variables (Blöschl et al. 1991; Guglielmin et al. 2003, 2022). Furthermore, the use of remotely sensed snow thickness data (Orsolini et al. 2019) or alternative models (Richter et al. 2019) would introduce additional uncertainties due to coarser ground resolutions, which are unsuitable for detecting the fine-scale variability of permafrost conditions.

The linear models were applied using the DEM as the independent variable. To better capture rapid changes, particularly in snow depth, regressions were calculated on a weekly basis rather than monthly, as was done in the original PERMACLIM (Guglielmin et al. 2003). This higher temporal resolution was applied to spring (March, April, May, June; MAMJ), when snowmelt initiates at different altitudes, and autumn (September, October, November; SON), when snow accumulation begins. Monthly steps were maintained only for summer (July and August; JA) and winter (December, January, February; DJF).

Snow depth is significantly influenced by physical phenomena such as wind (Mott et al. 2018) and solar radiation (Hock 1999), which are also mediated by topographical factors like concavity, convexity, and slope (Zhong et al. 2021). Compared to the original PERMACLIM, the effect of slope on snow distribution was updated to better account for accumulation due to avalanches. Specifically, the Snow Accumulation Factor (SAF) was upgraded by introducing a new function (R^2 = 0.97) for snow accumulation strictly within avalanche areas, identified via regional avalanche inventories (ARPA Lombardia 2024; Autonomous Province of Bolzano 2025; Autonomous Province of Trento 2025). This function applies to slopes between 12° and 24° (Table 1), with equations derived from data on snow thickness changes following avalanche events (Sovilla et al. 2010). The resulting snow thickening was added only downstream of the avalanche bodies. Outside of these designated areas, the original version of the SAF was retained (Guglielmin et al. 2003).

The curvature effect (CCF), which simulates wind erosion and deposition, has also been updated. In ridge areas where the curvature exceeds 0.02 m^{-1}, it is assumed that the ground surface remains snow-free (Blöschl et al. 1991). Both slope and curvature were calculated using the Surface Parameters module in ArcGIS Pro. The final snow depth correction was performed by multiplying the snow depth map by the SAF and the CCF (Step 1 – HS map). Remote sensing data were not utilized in this study, as snow depth is particularly difficult to assess using satellite techniques in rugged mountain regions (Santi et al. 2014). Furthermore, the coarse resolution (> 500 m/px) of typical remotely sensed snow depth products fails to represent the high spatial variability of heterogeneous Alpine topography. Additionally, such data require calibration with ground-truthing observations which, in this context, are provided by the AWSs. Consequently, we chose to directly model these ground observations at a higher resolution (10 m DEM) rather than relying on satellite-derived data.

While the selected AWSs may not capture the full environmental variability of the entire study area, restricting the study to a single pluviometric region (Pavan et al. 2019) and selecting all available stations with negligible missing data ensured a robust climatic harmonization of the dataset.

Moreover, the distribution of these AWSs covers the complete altitudinal range of the model domain. As a result, each AWS effectively represents the topographic context of its local area, which is accurately captured by the high-resolution pixels of the DEM (Cortez et al. 2020).

A third update to the snow distribution modelling was the introduction of a snow melting factor (M), adapted from the Hock formulation (Eq. 1) (Hock 1999, 2003):

Table 1 Updated snow accumulation factor (SAF) for the avalanche areas

Slope(x)	SAF
x≤12°	$-0.001x^2+0.0289x+0.8$
12° < x≤24°	$-0.001147x^3+0.047523x^2-0.568077x+2.954974$
24° < x≤42°	$-0.0006x^2+0.0021x+1.1435$
42° < x≤60°	$-0.0075x+0.6083$
x > 60°	0

$$M = \begin{cases} (MF + a_{snow} I)\,Ta & Ta > 0 \\ 0 & Ta \leq 0 \end{cases} \quad (1)$$

where MF is a melting factor (mm $day^{-1}°C^{-1}$), a_{snow} a radiation factor (m^2 mm W^{-1} h^{-1} $°C^{-1}$), I is the direct potential solar radiation under clear skies at the snow surface (W m^{-2}) and Ta is the air temperature (°C). When the incoming solar radiation is zero, the model corresponds to the classical degree-day approach. Considering that we want to calculate a representative melting of each temporal interval, for air temperature above 0 °C, the Hock's formulation adjusted for our study becomes (Eq. 2):

$$M = \left(\frac{MF}{24}LH + a_{snow}I_d + \frac{DDF}{24}DH\right)Ta \quad (2)$$

Where LH are the average light hours, DH are the average dark hours, I_d is the average direct potential solar radiation (kW h m^{-2}) and Ta is the average air temperature. Setting MF 1.8 mm day^{-1} °C, a_{snow} 0.6 10^{-3} m^2 mm W^{-1} h^{-1} $°C^{-1}$ and DDF 6.3 mm day^{-1} $°C^{-1}$ (Hock 1999) and converting M from millimetres of water to centimetres of snow the previous equation becomes (Eq. 3):

$$M = (0.075LH + 0.6I_d + 0.2625DH)\,Ta\frac{100}{\rho_{snow}} \quad (3)$$

Where ρ_{snow} is the snow density (kg m^{-3}). The snow melt is then subtracted from the snow depth maps previously corrected with SAF and CCF (Step 2 – HS final map). To improve the spatialization of the insulating effect of the snow, the model proposed by Jonas et al. 2009) to calculate snow density (ρ_{snow}) was used (Eq. 4):

$$\rho_{snow} = aHS + b + offset \quad (4)$$

Where ρ_{snow} is the snow bulk density (kg m^{-3}), HS is the snow depth in meters, a and b are regression coefficient dependent on elevation and time interval (Table 2). The offset for the study area is equal to −14.7 kg m^{-3}.

Table 2 Linear coefficient for estimating snow density with elevation above 2000 m a.s.l

Month	a	b
November	47	206
December	52	203
January	52	206
February	46	217
March	26	272
April	9	331
May	21	378
June	8	452
July	15	470

For the months of September and October, where regression coefficients are not available, the estimation of the snow bulk density was made according to Eq. 5 (Jonas et al. 2009):

$$\rho_{snow} = ((HS^{0.89})60.1) + 237 \quad (5)$$

Finally, the thermal conductivity of the snow was spatialized according to the model (Eq. 6) proposed by Sturm et al. (1997):

$$k_{eff} = \begin{cases} 0.138 - 1.01\rho_{snow} + 3.233\rho_{snow}^2 & 0.156 \le \rho_{snow} \le 0.6 \\ 0.023 + 0.234\rho_{snow} & \rho_{snow} < 0.156 \end{cases} \quad (6)$$

Where k_{eff} is the effective thermal conductivity of the snow ($W\ m^{-1}\ K^{-1}$) and ρ_{snow} is the snow bulk density ($g\ cm^{-3}$).

Updates to the PERMACLIM Model

Compared to the original version of PERMACLIM three main updates were carried out for the calculation of the GST:

a) When snow cover is present and the critical height (HC), as defined in the equation n. 2 of Guglielmin et al. (2003), is thinner of the HS the GST has been set equal to the GST of the previous period instead that 0 °C. The real GST below the snow should be improved by this update because the sensible heat flux (Qs, $W\ m^{-2}$) between the soil and the air is null in these conditions due to the insulating effect of the snow.
b) When snow cover is present and HS is thinner than HC, the Qs between soil and air, used for the GSTs computation, were re-calculated using all the stations available within the study area and outside, in the Italian Alps, for a total of 9 weather stations (Table 3), applying equation n. 1 in Guglielmin et al. (2003). The representative Qs for each period was calculated as the average of all sensible heat fluxes of all stations.
c) In snow free conditions, the GST is not more calculated as equal to the air temperature in the period from June to September, but it is computed considering the effect of solar radiation according to (Eq. 7) (Abramov et al. 2008; Guglielmin et al. 2008):

$$GST = Ta + \beta\, I_{tot} + \alpha \quad (7)$$

Where I_{tot} ($kW\ h\ m^{-2}$) is the total cumulative radiation calculated from the DEM with the tool Raster Solar Radiation of ArcGIS Pro software. β and α were estimated, for each time interval, from the linear relation between ΔT and I_{tot}, where ΔT = GST - Ta. The ΔT was calculated using the Ta

Table 3 AWS for sensible heat fluxes (Qs) estimation

Station name	Longitude	Latitude	Elevation(m)	Source
Alpe Cavallo	12° 6’ 41.39”	46° 40’ 16.29”	2345	Autonomous Province of Bolzano (https://meteo.provincia.bz.it)
Alpe del Tumulo	11° 8’ 55.23”	46° 54’ 48.86”	2230	Autonomous Province of Bolzano (https://meteo.provincia.bz.it)
Baldass	12° 34’ 30.88”	46° 14’ 53.3”	1817	ARPA Friuli-Venezia Giulia (https://www.osmer.fvg.it/home.php)
Giovo del Diavolo	10° 45’ 52.78”	46° 47’ 4.92”	3035	Autonomous Province of Bolzano (https://meteo.provincia.bz.it)
La Vallaccia	10° 11’ 19.98”	46° 28’ 38.21”	2660	ARPA Lombardia (https://www.arpalombardia.it)
Malga Fadner	11° 51’ 41.16”	46° 55’ 32.02”	2155	Autonomous Province of Bolzano (https://meteo.provincia.bz.it)
Monte Pratzen	10° 37’ 29.09”	46° 50’ 48.5”	2465	Autonomous Province of Bolzano https://meteo.provincia.bz.it)
Obereggen	11° 32’ 47.97”	46° 21’ 48.93”	2123	Autonomous Province of Bolzano https://meteo.provincia.bz.it)
Stelvio AWS ITEX	10° 26’ 26.88”	46° 31’ 53.4”	2612	Cannone unpublished data

values taken from the air temperature maps in correspondence of 10 selected ground surface thermistors placed in the study area.

Finally, all updates to the modelling of the GST compared to the original version of PERMACLIM are shown (in red) in Fig. 3.

The MAGST maps of the first (2020–2021) and second (2021–2022) hydrological year were obtained from the weighted average of the GST using the duration of each time interval as weights.

Since permafrost can develop also in area were MAGST is above zero (Smith e Riseborough 1996; Smith and

Riseborough 2002), Ikeda (2006) and (Abramov et al. 2008) proposed 2 °C as the maximum limit for the presence of permafrost conditions. Considering the upper limit of MAGST for permafrost conditions and the uncertainty of the average MAGST of ±0.5 °C, calculated according to Taylor's (2022) propagation theory, it is possible to set an upper limit for permafrost presence at 2.5 °C.

The MAGST maps were reclassified in order to identify areas where the surface conditions are favourable for the persistence of permafrost. According to the classification reported in Table 4, the model indicates whether the surface conditions are very favourable, favourable, slightly favourable or absent.

Model Validation and Comparison

The predictive performance of the models was evaluated using the Mean Absolute Error (MAE) and Root Mean Square Error (RMSE) (Willmott and Matsuura 2005; Chai and Draxler 2014; Hodson 2022). The correlation of the linear models was assessed using the Pearson index (r), while the goodness of fit was determined by the coefficient of determination (R^2) (Chicco et al. 2021). The validation of snow depth and air temperature maps was performed using data from the La Vallaccia, Madriccio, and Pian dei Cavalli weather stations (Fig. 1).

The average GST for each period and the MAGST maps for the first and second hydrological years were validated using data from 13 thermistors. These sensors were independent of those used for the extrapolation of the α and β coefficients and were located near Stelvio Pass, the Scorluzzo cirque, the Foscagno rock glacier, the La Vallaccia meteorological station, and the PACE borehole. For the La Vallaccia site (the only station in the validation set with concurrent measurements of Ta, GST, and HS) a temporal comparison was also conducted between measured and predicted values by calculating the RMSE and MAE.

To further evaluate its potential, the PERMACLIM 2.0 outputs for the 2020–2022 MAGST and permafrost conditions were compared with: (a) the TTOP formulation by Smith and Riseborough (1996), following the approach of Obu et al. (2019), with thawing and freezing n-factors calculated according to Gisnås et al. (2016); (b) the same TTOP formulation, but directly utilizing the ground thawing and freezing degree days calculated by PERMACLIM 2.0.

Software

The GIS procedure was implemented in R (version 4.5.1). Tabular data processing and graph creation were performed using Microsoft Excel (Microsoft 365), while cartographic production was carried out using QGIS (version 3.44.5).

Results

Air Temperature

Linear regression models for air temperature show a strong negative (or inverse) correlation ($-0.99 < r < -0.94$) between air temperature and elevation with an R^2 from 0.88 to 0.99. The elevation lapse rate ranges from −0.896 °C/100 m to −0.435 °C/100 m, with a mean value of −0.663 °C/100 m, for the hydrological year 2020–2021, and from −0.79 °C/100 m to −0.435 °C/100 m, with a mean value of −0.649 °C/100 m, for the hydrological year 2021–2022.

The mean annual air temperature (MAAT) for the first hydrological year is from −8.73 °C to 3.62 °C with a mean value of 0.25 °C. The MAAT for the second hydrological year is from −7.59 °C to 4.77 °C with a mean value of 1.40 °C. The overall MAE and RMSE for the hydrological year 2020–2021 are 0.64 °C and 0.83 °C, respectively, while the overall MAE and RMSE for the hydrological year 2021–2022 are 0.65 °C and 0.79 °C, respectively.

Snow Depth

Linear regression models for snow depth show a strong positive (or direct) correlation ($0.75 < r < 0.99$) between snow depth and elevation with an R^2 from 0.57 to 0.99. The lowest determination indices are related to the winter months while the highest at the onset of snowfall and during the melting period. The snow depth maps, validated after the application of the snow depth correction factors (slope effects, curvature effects and snow melting) show an overall MAE and RMSE for the hydrological year 2020–2021 of 17 cm and 26 cm, respectively, while for the hydrological year 2021–2022 show an overall MAE and RMSE of 9 cm and 15 cm, respectively. In the year 2020–2021, the snow season began, above 2700 m, in the first week of September and the snow lasted on the ground until the last week of June with snow only above 2900 m. In the year 2021–2022, the snow season began, above 2400 m, in the first week of October and the snow lasted on the ground until the second week of June above 3000 m, extending the snow-free period by more than 15 days compared to the previous year.

To better explain the improvements in snow distributions due to snowmelt correction, in Fig. 4a there is an example of snow distribution calculated by applying only slope and curvature corrections (SAF and CCF), while in Fig. 4b the snow map was corrected by also introducing snowmelt (M). The base map of PlanetScope represents

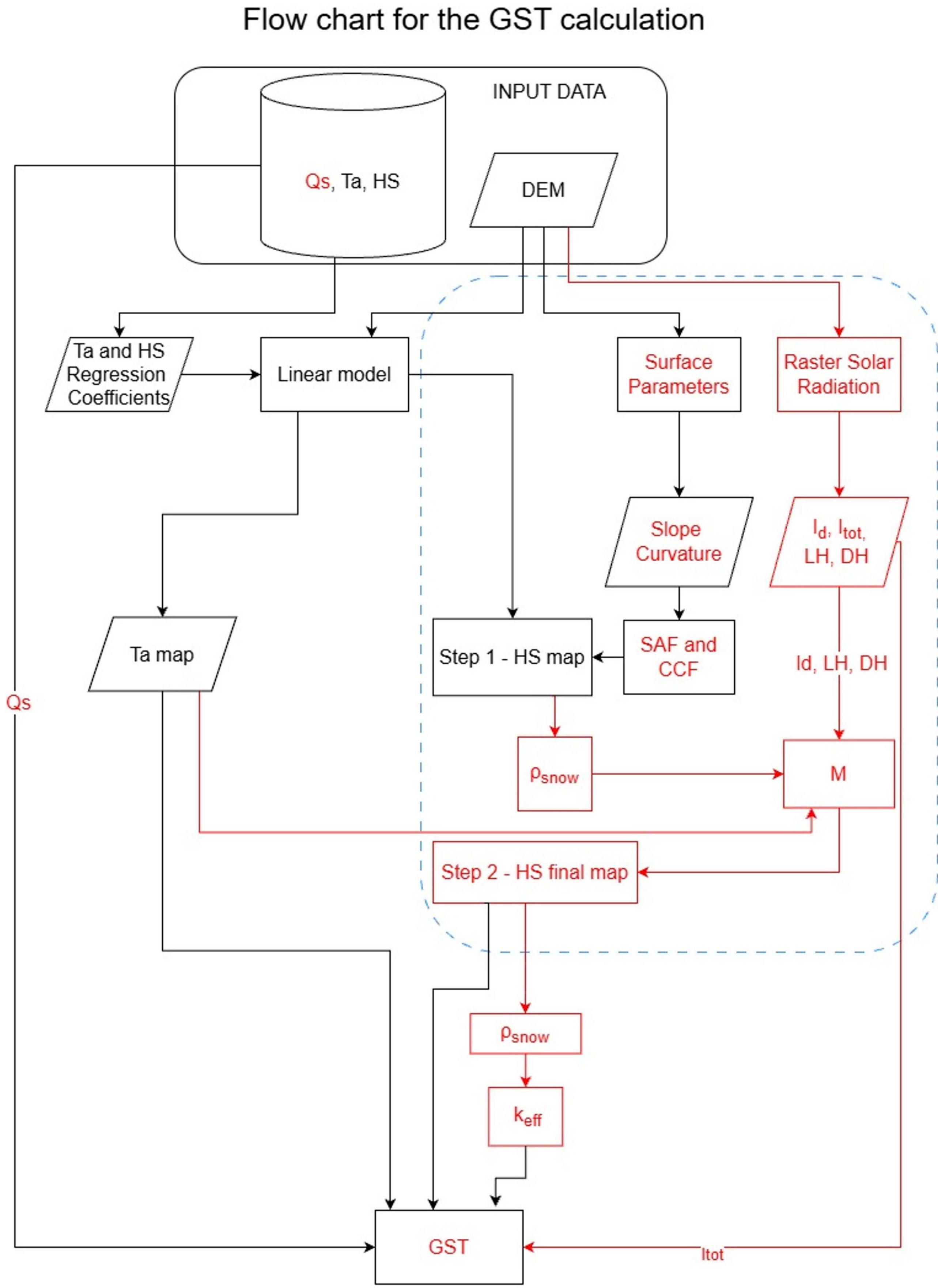
Flow chart for the GST calculation
INPUT DATA
Qs, Ta, HS
DEM
Ta and HS Regression Coefficients
Linear model
Surface Parameters
Raster Solar Radiation
Slope Curvature
Id, Itot, LH, DH
Ta map
Step 1 - HS map
SAF and CCF
Id, LH, DH
Qs
ρsnow
M
Step 2 - HS final map
ρsnow
keff
GST
Itot

Fig. 3 Simplified flow chart for the GST calculation with updates (in red). The red boxes and arrows indicate a new process, while the red words indicate a calculation that was contained in the previous version of PERMACLIM but has been updated. The light-blue dotted polygons include all the procedures for the calculation of HS map. Ta, HS, Qs and the DEM are the main inputs of the model. Regression coefficients of Ta and HS are applied in the in the linear model using DEM as prediction variable. Surfaces Parameters and Raster Solar Radiation are tools of ArcGIS Pro. SAF and CCF are, respectively, the slope and curvature corrections for the snow map (Step 1 – HS map). I_d, I_{tot}, LH, DH and ρ_{snow} are the input for the calculation of M used for the correction of the snow map (Step 2 – HS final map). The GST is the final output of the model. This process has been implemented for each time interval

the real distribution of the snow of the 27th of May 2022 (the only available clear sky satellite scene during the snow melting season) at the Stelvio Pass during the melting season. The snow map in Fig. 4b shows a more reliable snow distribution compared to Fig. 4a. In fact, accounting for snowmelt allows for more realistic snow-map boundaries to be defined. This approach emphasizes the differences between north- and south-facing slopes and eliminates residual snow patches in convex areas, leading to a more accurate representation of the landscape.

Snow depth corrections have a strong impact also on the physical properties of the snow, like density (ρ_{snow}) and thermal conductivity (k_{eff}), which are directly affected by snow depth. In Fig. 5 it is reported an example at the Stelvio Pass, for January 2021, between a snow depth map without (Fig. 5a) and with (Fig. 5b) snow depth corrections and the effects on snow density (Fig. 5c) and snow thermal conductivity (Fig. 5d). From the image it is possible to observe the similar distribution patter of snow depth, snow density and snow thermal conductivity.

Ground Surface Temperature

The regression models used to calculate α and β coefficients for the GST estimation during the snow-free period (Eq. 7)

Table 4 Permafrost conditions: very favourable, favourable, slightly favourable and absent

		MAGST 20–21 (°C)			
		(-∞; 0]	(0; 2]	(2; 2.5]	(2.5; +∞)
MAGST 21–22 (°C)	(-∞; 0]	very favourable	favourable	slightly favourable	absent
	(0; 2]	favourable	favourable	slightly favourable	absent
	(2; 2.5]	slightly favourable	slightly favourable	slightly favourable	absent
	(2.5; +∞)	absent	absent	absent	absent

always show a correlation index higher than 0.7, indicating a strong positive relation between the solar radiation and the GST, and an R^2 always above 0.5 which increases for the month of July and August and for the weeks of September until 0.9, where many points are snow free. Validation carried out with 13 thermistors for the hydrological year 2020–2021 (see Sect. 4.3) returns an overall MAE and RMSE of 0.7 °C and 1.38 °C, respectively, while for the hydrological year 2021–2022 the overall MAE and RMSE are 1.09 °C and 1.77 °C, respectively.

Air Temperature, Snow Depth and Ground Surface Temperature Over time

Unlike the previous version of the model, which generated monthly mean air temperature and snow depth maps by averaging 10-year values, the updated version calculates these maps for each individual time step. Consequently, it is now possible to obtain a GST value for every time interval. Figure 6a and b, and 6c illustrate the trends between measured and modelled values for Ta, HS, and GST, respectively, at the La Vallaccia station (the only AWS within the study area providing all three parameters). The HS and GST charts also include a comparison between the original model and the updated version, specifically highlighting: HS values with and without snow depth corrections; GST values with and without snow depth corrections and the radiative correction factor during the snow-free period. For these time series, MAE and RMSE were calculated based on the residuals between measured and modelled values, while the coefficient of determination (R^2) was used to assess the correlation between predicted and observed data.

The corrections applied to snow modelling increased the predictive power of the model (Fig. 6b). The MAE, for the first hydrological year, changed from 31 cm to 21 cm with a reduction of the 30%, while the RMSE changed from 38 cm to 27 cm with a reduction of the 29%. The MAE, for the second hydrological year, changed from 15 cm to 11 cm with a reduction of the 26%, while the RMSE changed from 22 cm to 18 cm with a reduction of the 18%. In Fig. 6c it is reported the modelled GST with and without any corrections respect to the measured values. The MAE, for the first hydrological year, changed from 0.92 °C (without corrections) to 0.60 °C while the RMSE changed from 1.40 °C (without corrections) to 1.17 °C with an improvement of 35% and 17%, respectively. The MAE, for the second hydrological year, changed from 1.80 °C to 0.9 °C with a reduction of the 50%, while the RMSE changed from 2.51 °C to 1.29 °C with a reduction of the 49%. In terms of R^2 the results remain substantially unchanged, with an R^2 always above 0.9.

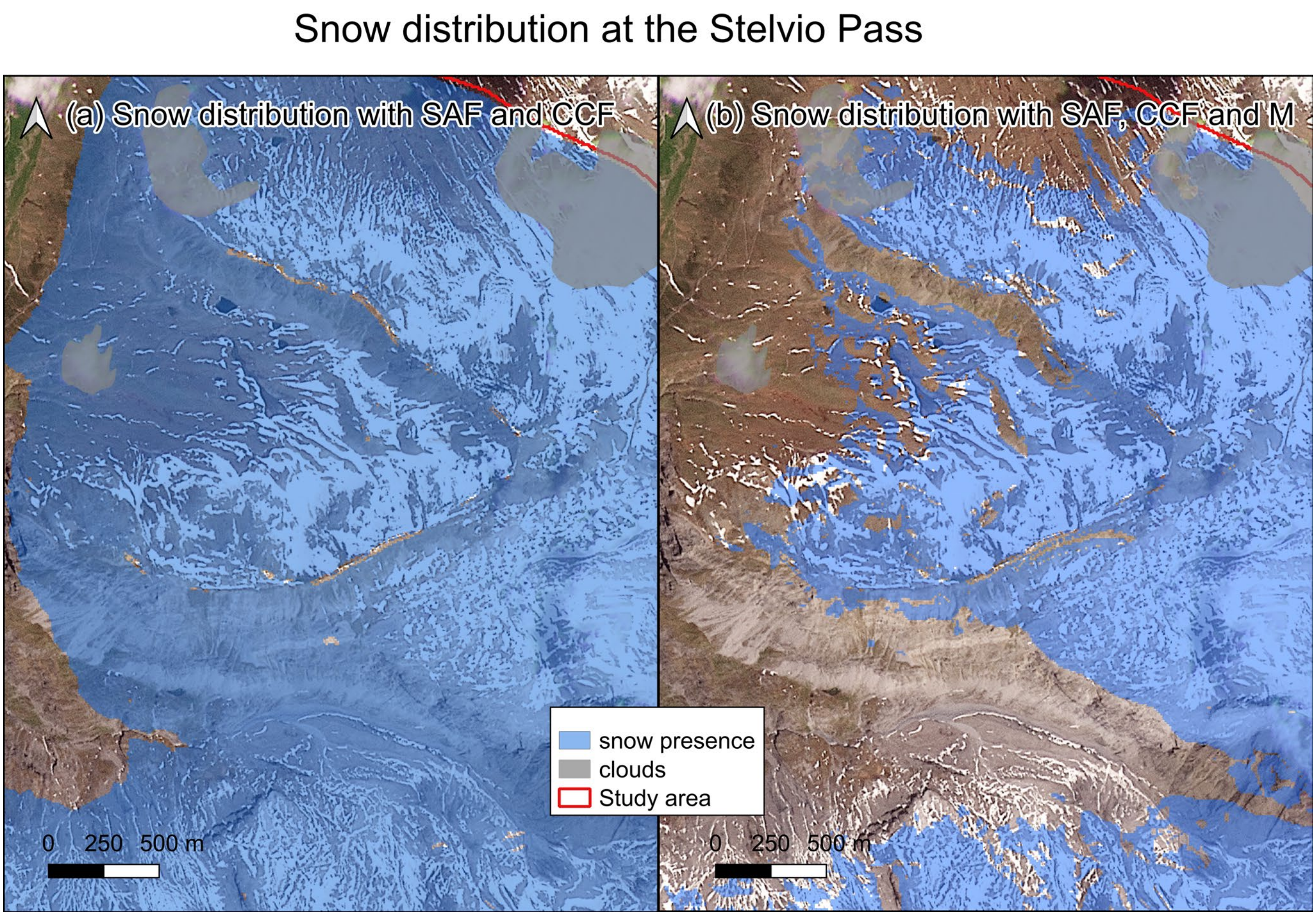

Fig. 4 Snow distribution map at the Stelvio Pass corrected with SAF and CCF **(a)** and snow map distribution corrected with SAF, CCF and M **(b)**. The base map is a satellite Planet Scope scene of the 27th of May 2022 representing the real snow distribution. Grey polygons represent clouds, while the red line is the border of the study area

Mean Annual Ground Surface Temperature

Another key result are the maps of MAGST for the first (2020–2021) and second (2021–2022) hydrological years. To appreciate the differences between the two years, a zoom on the Stelvio Pass area is reported (Fig. 7). In Fig. 7 it is shown also a comparison between the MAAT and the MAGST for both years. The MAAT of the first year is colder than the second year and therefore the MAGST of the first year is lower than that of the second year. More in details, the MAGST for the first hydrological year ranges from −8.6 °C to 5.8 °C with a mean value of 2.1 °C. The MAGST for the second hydrological year ranges from −7.4 °C to 6.7 °C with a mean value of 3 °C.

The simulations performed with PERMACLIM 2.0 yield more reliable results compared to the previous version of the model. For the first hydrological year, the predictive power improved in terms of MAE and MAGST by 45% and 34%, respectively. During the second hydrological year, improvements reached 50% and 48% (Table 5).

Permafrost Conditions Map

Using the reclassification procedure presented in Table 4 (see Sect. 4.2), it is possible to obtain a map of the permafrost conditions for the hydrological biennium 2020–2022, highlighting areas with very favourable, favourable, slightly favourable and absent permafrost conditions. In Fig. 8 it is reported a zoom in on the Stelvio Pass area, where it is possible to observe the typical patched pattern of permafrost in alpine regions.

In Fig. 9 it is presented a map of the permafrost conditions of the entire study area with a spatial resolution of 10 m. The extensions of glaciers, uploaded to the most recent available version, were downloaded from the geoportals of the Lombardia Region (Regione Lombardia 2016), Autonomous Province of Bolzano (2017) and Autonomous Province of Trento (2015).

Across the entire study area (Fig. 9), 67.8% of the territory exhibits unfavourable permafrost conditions, while just over 25% presents slightly favourable or favourable

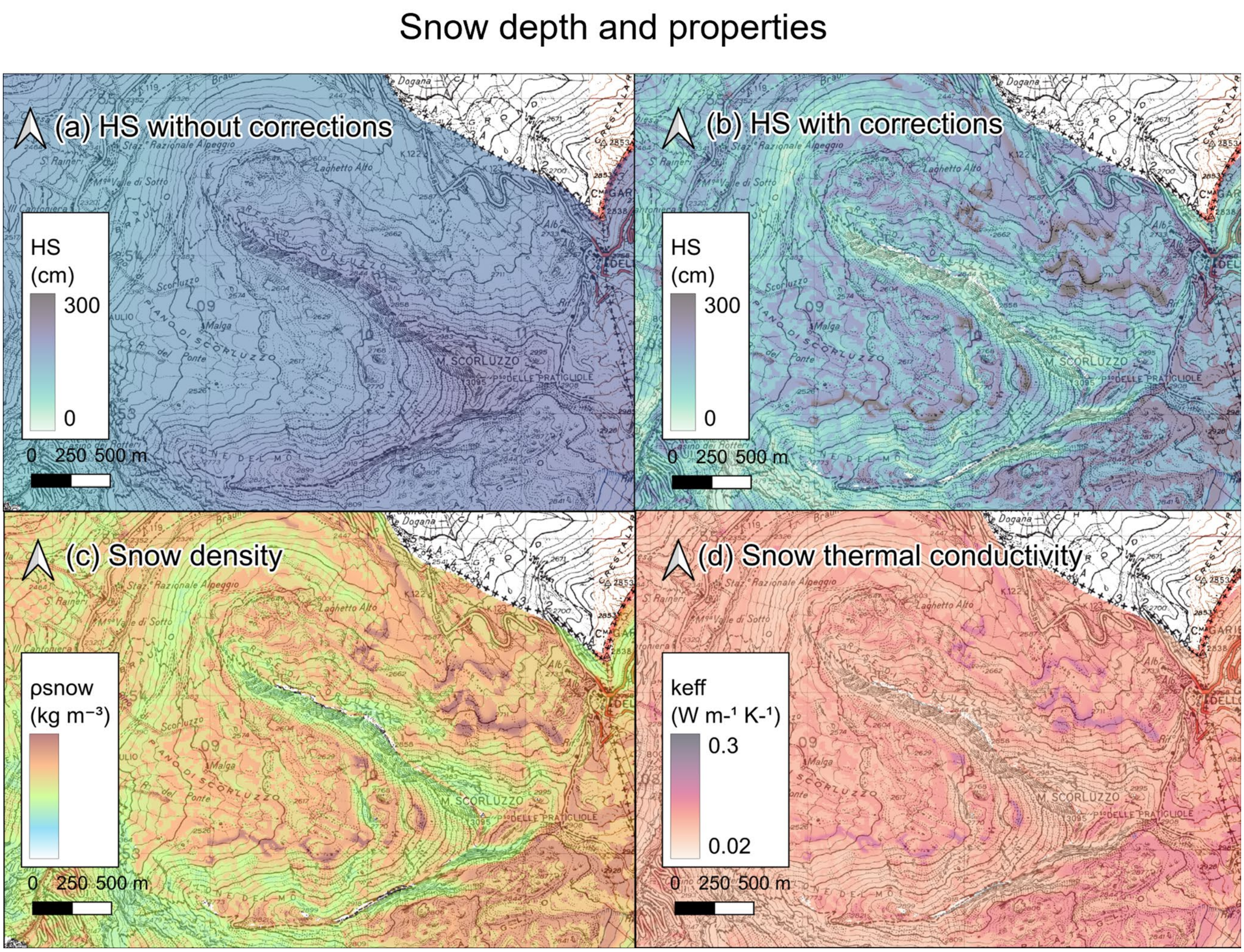

Fig. 5 Comparison between the HS maps without **(a)** and with **(b)** snow depth corrections and the snow density **(c)** and the snow thermal conductivity **(d)**, at the Stelvio Pass, for January 2021. The base map is provided by the Istituto Geografico Militare (IGM) through the Italian National Geoportal WMS service (1:25,000) (https://gn.mase.gov.it/portale/servizio-di-consultazione-wms)

conditions. Only 6.2% of the area shows very favourable conditions. Notably, for the examined period, very favourable conditions are never found below 2400 m a.s.l.

Discussion

Considerations on Modelling Climate Variables

Air temperature is a climatic variable that, in mountainous regions with complex topography (i.e. Amin et al. 2024), is often modelled using various techniques, including multiple linear regression, Inverse Distance Weighting (IDW), and different kriging approaches (Chuanyan et al. 2005; Benavides et al. 2007). In this study, we demonstrate that simple linear regression models based on elevation are an effective tool for modelling average air temperature over time without increasing computational costs (Ponti et al. 2020; Guglielmin et al. 2022; Chaturvedi et al. 2026). The observed temperature gradients indicate that air temperature inversion phenomena are not evident on weekly or monthly timescales, proving that a linear model (elevation lapse-rate) is sufficient to describe temperature variability.

Previous studies report RMSE values for air temperature between 1.2 and 1.9 °C for partially glacierized areas of the Swiss Alps (Magnusson et al. 2011), and approximately 0.64 °C for large-scale heterogeneous Alpine terrain (Fiddes et al. 2015), highlighting the comparable performance of the PERMACLIM model (see Sect. 5.1).

Snow modelling is a complex challenge that has led to the development of increasingly sophisticated tools for predicting, among other things, avalanche risk. Snowpack (Lehning et al. 1999) and Alpine 3D (Lehning et al. 2006) are among the most advanced models for simulating

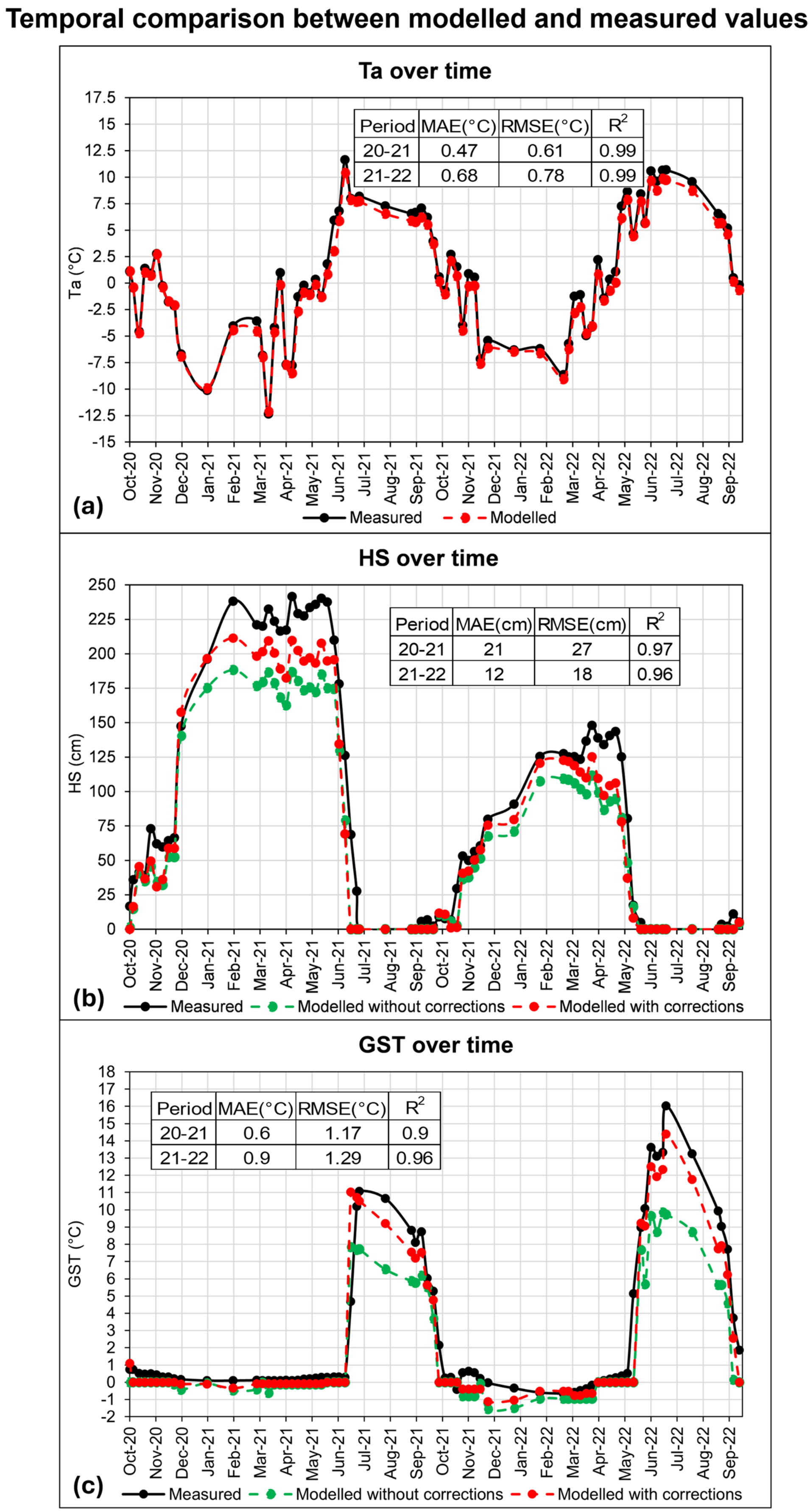

Fig. 6 Temporal comparison between the modelled with all the corrections (red line) and measured (black line) values of Ta **(a)**, HS **(b)** and GST**(c)**, at La Vallaccia site, of the hydrological biennium 2020–2022. The green dashed lines indicate the modelled values of HS and GST without correction factors

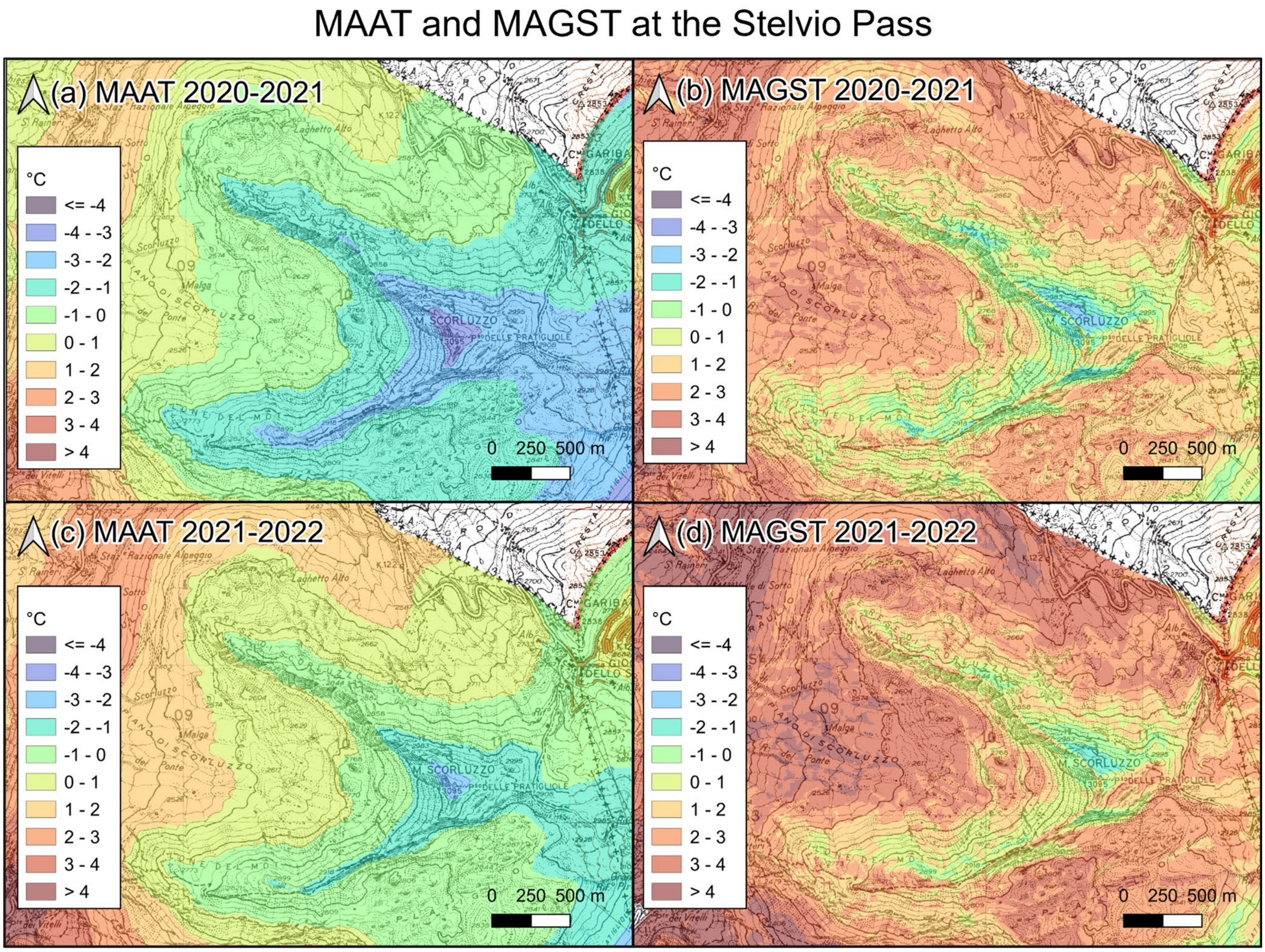

Fig. 7 Comparison between the MAAT and the MAGST at the Stelvio Pass for the first and second hydrologic year. **(a)** and **(b)** represent the MAAT and the MAGST of the hydrologic year 2020–2021, while **(c)** and **(d)** represent the MAAT and the MAGST of the hydrological year 2021–2022. The base map is provided by the Istituto Geografico Militare (IGM) through the Italian National Geoportal WMS service (1:25,000) (https://gn.mase.gov.it/portale/servizio-di-consultazione-wms)

Table 5 validation of the MAGST and comparison with the previous PERMACLIM

Period	PERMACLIM			PERMACLIM 2.0		
	MAE (°C)	RMSE (°C)	R^2	MAE (°C)	RMSE (°C)	R^2
2020–2021	0.82	0.91	0.40	0.45	0.60	0.74
2021–2022	1.22	1.55	0.44	0.61	0.80	0.77

snowpack thickness and properties in the Alps. However, the temporal resolution of the data and the number of variables required for these simulations exceed those available for this study. Therefore, simple linear regression models based on elevation, corrected with topographic factors as proposed by several authors (Blöschl et al. 1991; Guglielmin et al. 2003, 2022; Chaturvedi et al. 2026), serve as a valuable tool for generating snow depth maps. Analysis of residuals and coefficients of determination (R^2) shows that these simple linear models effectively predict snow depth during autumn and spring, though they are less accurate during winter.

During the winter period, snow depth curves relative to altitude typically increase to a maximum value before decreasing at higher elevations (between 2800 and 3000 m a.s.l.). This was particularly evident during the 2021–2022 hydrological year, when cumulative snowfall was lower than the previous year. This is the most common accumulation pattern, with 79% of sub-catchments exhibiting this trend (Grünewald et al. 2014). This phenomenon can be

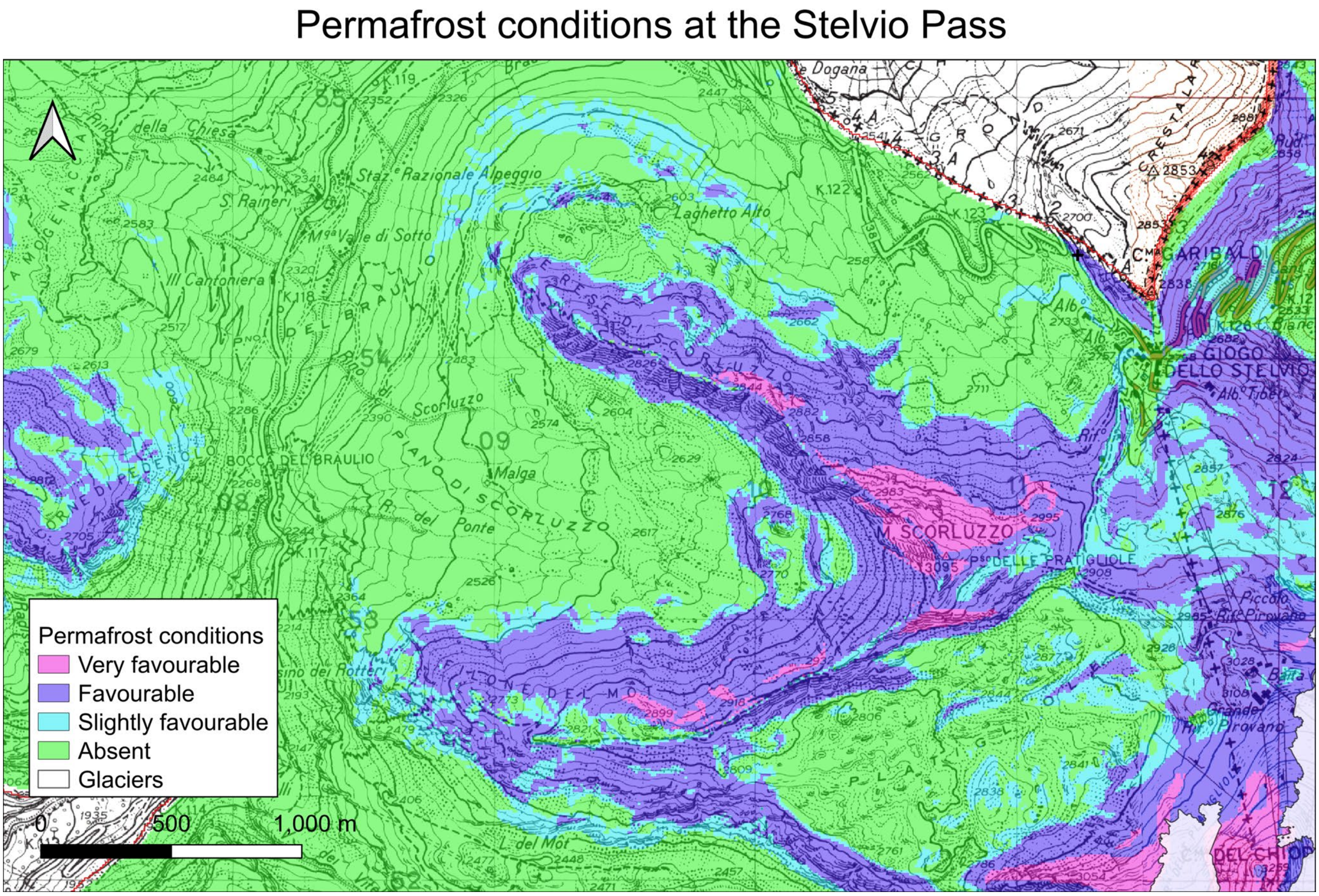

Fig. 8 Permafrost conditions map at the Stelvio Pass for the hydrological biennium 2020–2022. The base map is provided by the Istituto Geografico Militare (IGM) through the Italian National Geoportal WMS service (1:25,000) (https://gn.mase.gov.it/portale/servizio-di-consultazione-wms)

explained by the Clausius–Clapeyron effect (Roe and Baker 2006): the decrease in temperature and air density with altitude reduces the atmosphere's capacity to retain water vapour. Consequently, above a certain altitude, the reduction in moisture availability outweighs the increased condensation from adiabatic cooling, leading to a decrease in high-altitude precipitation. Alternatively, Grünewald et al. (2014) suggested that the primary factors affecting snow depth at high altitudes are wind and gravity, which redistribute snow from steep, exposed areas to more sheltered, gentle slopes at lower altitudes. This explains why the empirical correction factors in our model, designed to simulate wind erosion/accumulation (CCF) and gravitational phenomena (SAF), improve simulation results compared to the linear model alone (Fig. 6b).

Accounting for snowpack melt has improved the predictive power of the linear models by eliminating excess snow in areas most exposed to solar radiation, resulting in a more realistic distribution pattern (Fig. 4b). Beyond topographic factors like slope and concavity, snowpack rearrangement can be simulated by considering wind action. The main factors related to wind are saltation, turbulent suspension, and sublimation, which are primarily functions of wind speed, aerodynamic roughness, air temperature, and relative humidity (Pomeroy and Gray 1990; Liston and Sturm 1998). Mass conservation models, such as the MTD (Gruber 2007) or SnowSlide (Bernhardt and Schulz 2010), can also simulate snow movement.

However, implementing such elaborate models is beyond the current scope of this work, as we aim for broad and simple reproducibility of the proposed update. Many necessary variables, such as vegetation maps with aerodynamic roughness and snow-holding capacity attributes, are unavailable. Additionally, these models are typically designed for catchment scales and would require adaptation for regional use. Consequently, linear models with empirical correction factors represent a robust alternative. Indeed, the simulations proposed here (see Sect. 5.2) show performances comparable to other regional-scale modelling approaches based on the Crocus snow model, such as SURFEX/ISBA–Crocus in southern Norway (Luijting et al. 2018) (RMSE: 27–62 cm) and the SAFRAN–SURFEX/ISBA–Crocus chain in the French Alps (Vionnet et al. 2019) (RMSE: 24–51 cm above 2000 m a.s.l.).

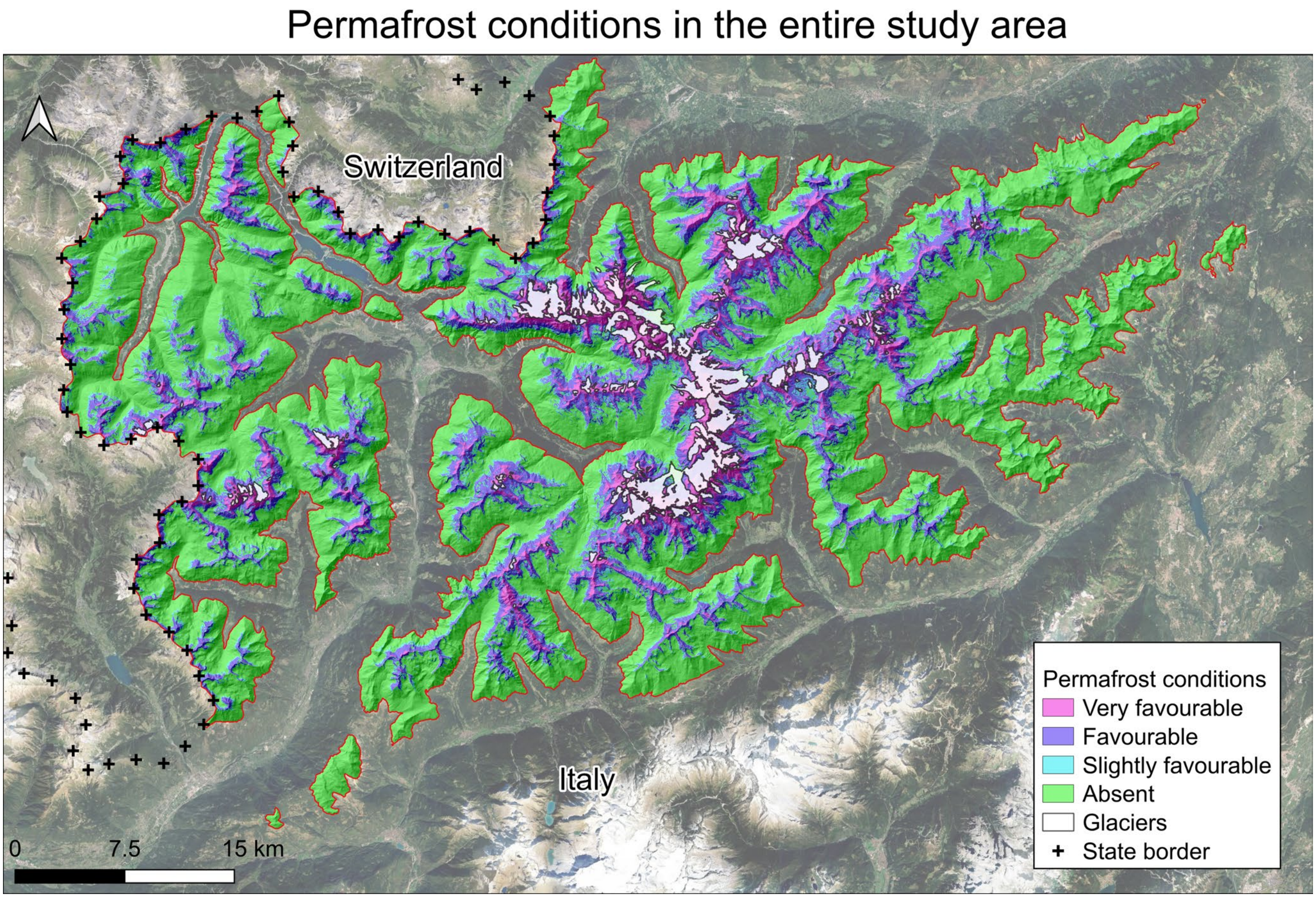

Fig. 9 Permafrost conditions map for the entire Upper Valtellina and neighbouring Trentino-Alto Adige territory. As base map was used a satellite image of Google Maps

As shown in Fig. 6c, the corrections proposed for the summer (which include radiative effects) are an order of magnitude greater than those for snow cover, which accounted for only 8% in 2020–2021 and 3.4% in the following year. Nevertheless, in areas characterized by strong winds and significant snow drifting, the impact of GST improvements during the snow-free period is more limited (Fig. 10). This is observed at the PACE borehole site, where extreme wind effects during the snow season, demonstrated by gusts exceeding 100 km/h that have repeatedly destroyed the station's anemometer (Guglielmin, personal communication), result in a much thinner snowpack than expected. Detailed modelling of wind-driven snow redistribution remains outside the scope of this research, as snow depth is treated here as an input variable to ultimately explain GST distribution.

PERMACLIM and Other Models

Since PERMACLIM 2.0 is a physics-based model whose primary outputs are MAGST values, its predictive power can only be evaluated by comparing measured and predicted values, as detailed in Sect. 5.4. The validation demonstrates that PERMACLIM 2.0 produces reliable results consistent with existing literature. Indeed, our RMSE (ranging from 0.6 °C to 0.8 °C) is comparable to models such as CryoGRID version 1.0, which yields MAGST maps with an overall RMSE of 1.2 °C (Gisnås et al. 2013) or 1.3 °C (Gisnås et al. 2016) when applied to Norway.

Regional simulations in an area very similar to our study site (the Swiss Alps) show an RMSE for MAGST on non-bedrock surfaces between 0.67 °C and 1.34 °C (Fiddes et al. 2015). The strong performance of PERMACLIM can also be attributed to the spatial resolution of the data; using a DEM with a 10-meter resolution yields more accurate validation results. These findings also suggest that models based on full energy balances are not always strictly necessary for calculating MAGST (Gruber 2005), as high-quality results can be achieved with simpler tools.

Conversely, the newly proposed classification for mapping permafrost conditions cannot be tested directly.

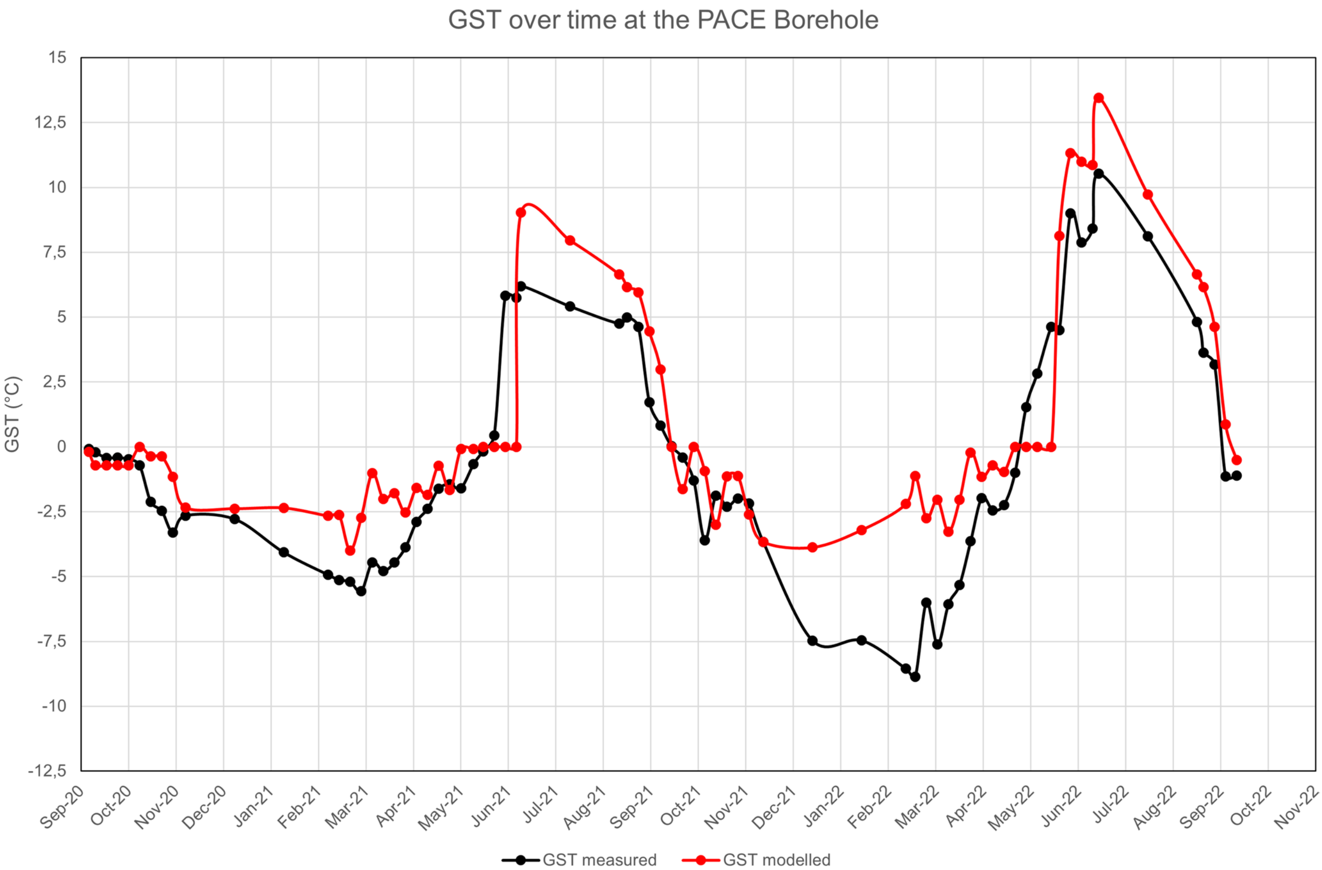

Fig. 10 Comparison between the measured (black line) and the modelled GST with all the corrections proposed for PERMACLIM 2.0 (red line) at the PACE borehole (3000 m asl, see Fig. 11). At this site the winter winds can easily exceed 100 km/h and the snow is generally thinner of what expected with an overestimation of the snow modelling and of the GST

However, it is possible to compare it with other models that illustrate permafrost distribution in terms of probability (Fig. 11). Specifically, the PERMACLIM 2.0 results can be compared with: (a) the TTOP formulation by Smith and Riseborough (1996), using n-factors for thawing and freezing calculated according to Gisnås et al. (2016); (b) the same TTOP formulation, but directly utilizing the ground thawing and freezing degree days calculated by PERMACLIM 2.0. For the former, the phytosociological map by Malfasi and Cannone (2021) and the geological map of the Stelvio Pass (Montrasio et al. 2012) were used for land-use classification, while thermal conductivity ratios were sourced from Obu et al. (2019). In both cases, the probability of occurrence was calculated following the procedure of Wang et al. (2023).

Among the three models, PERMACLIM 2.0 shows the best agreement with geophysical investigations of cryotic active landforms in the study area (Pavoni et al. 2026), demonstrating that the classification proposed in Table 4 is both realistic and applicable. Specifically, Fig. 11c illustrates a spatial distribution of permafrost conditions on the upper section of the active rock glacier at the Stelvio Pass (RGSP, Pavoni et al. 2026) and the frontal part of the Scorluzzo rock glacier (RGS, Sannino et al. 2021). In contrast, the TTOP models (Fig. 11a and b) indicate no permafrost probability within these rock glacier boundaries. It is also noteworthy that, in the relict rock glacier at Le Rese di Scorluzzo (RGRS) and the adjacent relict protalus rampart (PRRS), the PERMACLIM 2.0 results align well with the geophysical data from Pavoni et al. (2026), which indicated the presence of permafrost despite their geomorphological classification as relict; the TTOP models, however, indicate an absence of permafrost.

The agreement between the model and field measurements is even more pronounced at the only available borehole (PACE B, Guglielmin et al. 2018; Etzelmüller et al. 2020; Noetzli et al. 2025). At this site, permafrost exists and the model predicts "favourable" permafrost conditions, whereas the TTOP models show no likelihood of permafrost. Figure 12 displays the thermal envelope of the PACE borehole for the first 20 m between 2020 and 2024. The

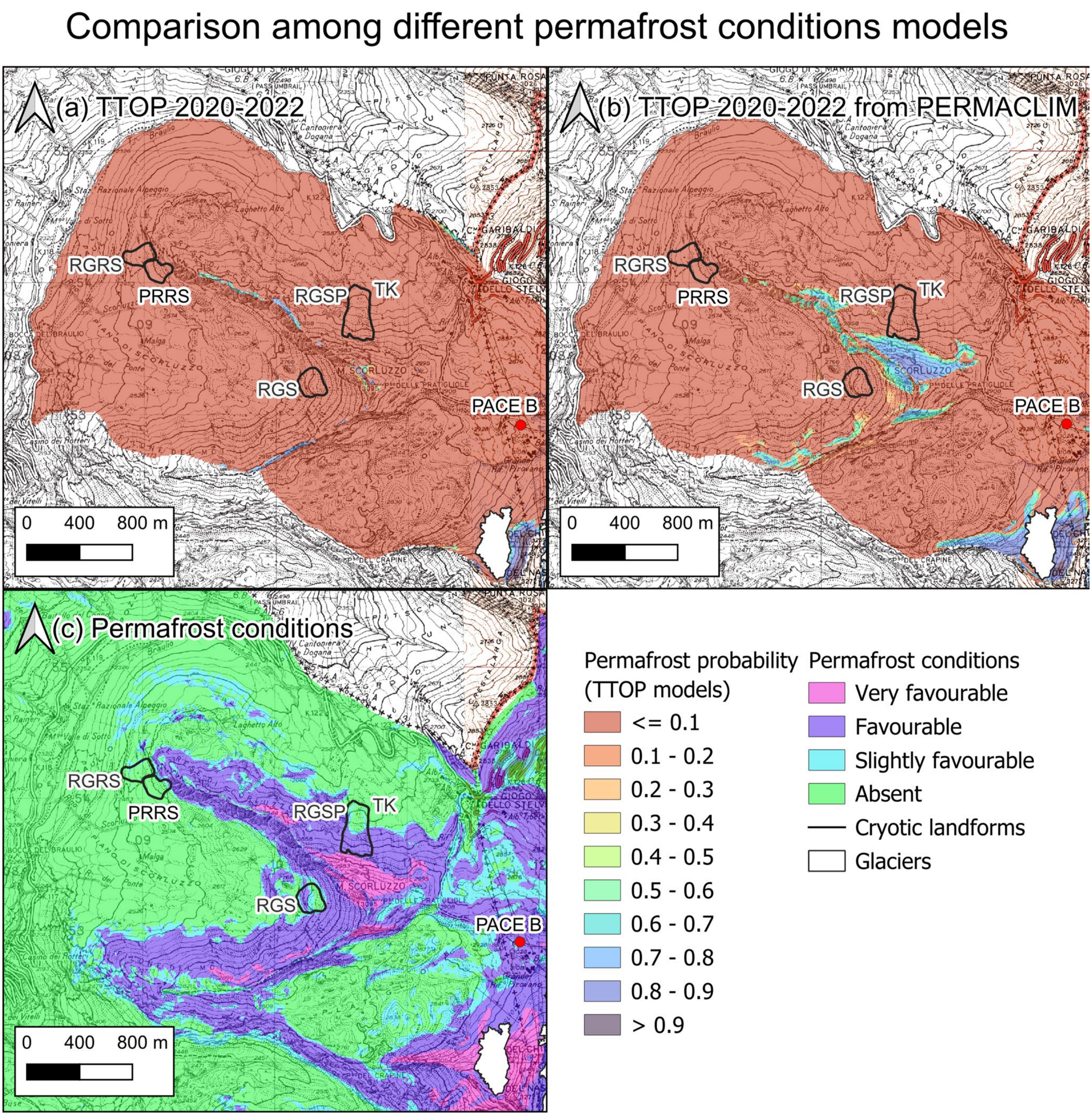

Fig. 11 Comparison among **(c)** the permafrost conditions map obtained from PERMACLIM 2.0 and two different versions of the TTOP model **(a**, **b)**, obtained from the same climatic variables, for the hydrological biennium 2020–2022. The figure shows also the most studied cryotic landforms present in the study area. The rock glacier at Le Rese di Scorluzzo (RGRS), the adjacent protalus rampart (PRRS) and the rock glacier at the Stelvio Pass (RGSP) have recently been investigated using geophysical methods by Pavoni et al. (2026). The thermokarst area (TK) was studied by Guglielmin et al. (2021), while the rock glacier at Scorluzzo (RGS) by Sannino et al. (2021). In Fig. 12 it is also reported the borehole of the Permafrost and Climate in Europe project (PACE B). The base map is provided by the Istituto Geografico Militare (IGM) through the Italian National Geoportal WMS service (1:25,000) (https://gn.mase.gov.it/portale/servizio-di-consultazione-wms)

measured MAGST for the two years considered was −0.8 °C and −0.5 °C, respectively; the permafrost condition map indicates "favourable" conditions according to Table 4, as the modelled MAGST was 0 °C and 1.3 °C.

Finally, it is interesting to observe that PERMACLIM 2.0 and both TTOP models correctly predict the absence of permafrost in the thermokarst area described by Guglielmin et al. (2021).

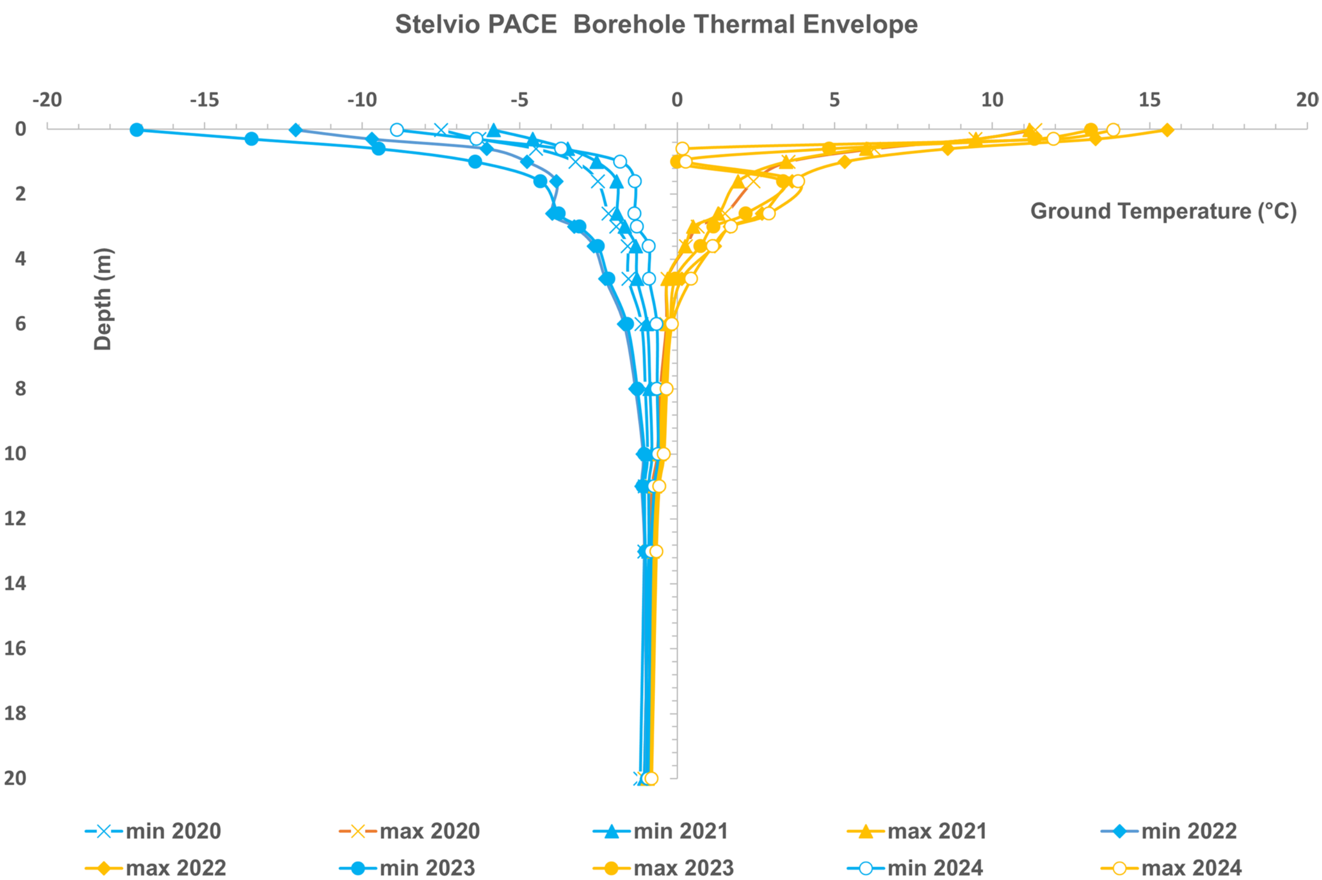

Fig. 12 Thermal envelope at PACE Borehole (3000 m asl) between 2020 and 2024

Applications of PERMACLIM 2.0

The GST values obtained with PERMACLIM 2.0 can be readily applied to calculate active layer thickness. Furthermore, the snow depth and snowmelt maps can be integrated into hydrological balance models at the basin scale, such as COSERO (Frey and Holzmann 2015), or at the regional scale, using tools like the BIGBANG model (Braca et al. 2022).

Characterizing permafrost conditions is essential for risk assessment, particularly in developing vulnerability maps for mountain areas facing climate change, which are particularly susceptible to topographic variations (Bickel and Manconi 2022). To address this, we propose a permafrost vulnerability map derived from the intersection of the existing Alpine Permafrost Index Map (APIM, Boeckli et al. 2012b) and the permafrost condition map presented in this study, applying the criteria outlined in Table 6.

The resulting vulnerability map highlights areas where specific management or mitigation strategies are required (Fig. 13). Indeed, rapid changes in permafrost distribution and thermal properties can significantly impact local infrastructure (Hjort et al. 2022) and the landscape (Duvillard et al. 2019; Guglielmin et al. 2021). As shown in Fig. 13, the PACE B site is characterized by minimum vulnerability; this is consistent with the borehole's warming rate, which is less pronounced than those recorded in other boreholes across the Central and Eastern Alps (Etzelmüller et al. 2020;

Table 6 Cryospheric vulnerability rules: permafrost and glacier vulnerability increases as the degree of "favourable" permafrost conditions (defined by PERMACLIM 2.0) decreases, and as the probability of permafrost occurrence (defined by APIM classes) increases

		Permafrost conditions			
		Very Favourable	Favourable	Slightly Favourable	Absent
APIM	**Permafrost in nearly all conditions**	No	Minimum Vuln.	Medium Vuln.	High Vuln.
	Permafrost mostly in cold conditions	No	No	Minimum Vuln.	Medium Vuln.
	Permafrost only in very favorable conditions	No	No	No	Minimum Vuln.
	No permafrost	No	No	No	No
	Glaciers	No	Minimum Vuln.	Medium Vuln.	High Vuln.

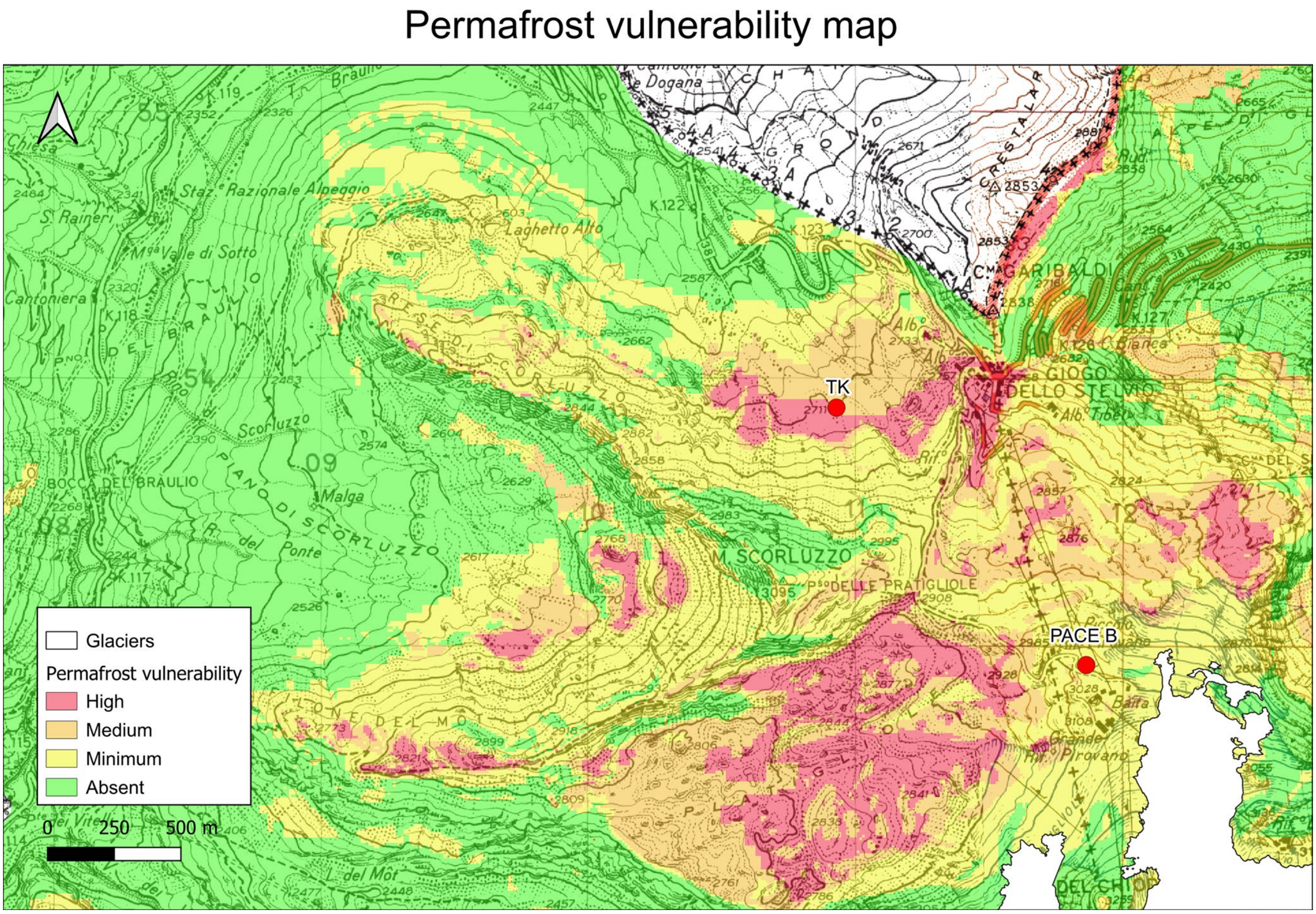

Fig. 13 Permafrost vulnerability map obtained intersecting the APIM and the Permafrost conditions map. The base map is provided by the Istituto Geografico Militare (IGM) through the Italian National Geoportal WMS service (1:25,000) (https://gn.mase.gov.it/portale/servizio-di-consultazione-wms)

Noetzli et al. 2025). Conversely, the thermokarst area is characterized by high vulnerability.

Conclusions

PERMACLIM 2.0 is a new tool designed to calculate MAGST at a spatial resolution of 10 m on a local-to-regional scale. Simulation results demonstrate that the model can predict MAGST with high accuracy using only simple, readily available input data. The model also provides spatialized outputs for each time interval, including maps of average air temperature, snow depth, snowmelt, snow density, and snow thermal conductivity.

Validation of air temperature, snow depth, and ground surface temperature yielded results consistent with published literature. These findings demonstrate that the updates implemented in this version significantly improve MAGST calculations compared to the previous PERMACLIM release, showing superior performance even when compared to other ground temperature models, such as TTOP.

The resulting permafrost condition maps identify areas where conditions are very favourable, favourable, or slightly favourable. This information can be easily updated with new data every one or two years, providing a dynamic tool to assess vulnerability to hazards and risks within the current climate change scenario.

Author contributions M.G. Supervised the work, found the funding, revised the draft of the work; E.R. wrote the first draft and prepared all the figures and made almost all the analyses; S.P. revised the draft and partially contributed to the data analyses.

Funding Open access funding provided by Università degli Studi dell'Insubria within the CRUI-CARE Agreement.

Data Availability Any new data produced through the data analyses of this paper will be available on request to the corresponding author.All the climate data used coming from public and private instituions are cited in the paper and can be requested directly to these organizations.

Declarations

Competing interests The authors declare no competing interests.

References

Abramov A, Gruber S, Gilichinsky D (2008) Mountain permafrost on active volcanoes: field data and statistical mapping, Klyuchevskaya volcano group. Kamchatka Russia Permafr Periglac 19:261–277. https://doi.org/10.1002/ppp.622

Amin G, Imtiaz I, Haroon E, Saqib NU, Shahzad MI, Nazeer M (2024) Assessment of machine learning algorithms for land cover classification in a complex mountainous landscape. J Geovisualization Spat Anal 8(2):34. https://doi.org/10.1007/s41651-024-00195-z

ARPA Lombardia (2024) Carta di Localizzazione probabile delle Valanghe (CLPV). Geoportale della Lombardia. https://www.geoportale.regione.lombardia.it

Autonomous Province of Bolzano (2017) Catasto dei ghiacciai. Geocatalogo della Provincia Autonoma di Bolzano. https://siat.provincia.tn.it/geonetwork/srv/ita/catalog.search#/home

Autonomous Province of Bolzano (2025) LAKA – Catasto valanghe. Hazard Browser provincia di Bolzano. https://pericoli-naturali.provincia.bz.it/it/hazard-browser

Autonomous Province of Trento (2017) Ghiacciai. WebGIS della Provincia Autonoma di Trento. https://webgis.provincia.tn.it/

Autonomous Province of Trento (2025) Carta pericolosità valanghe. Geocatalogo della Provincia Autonoma di Trento. https://siat.provincia.tn.it/geonetwork/srv/ita/catalog.search#/home

Bartolini E, Claps P, D'Odorico P (2009) Interannual variability of winter precipitation in the European Alps: relations with the North Atlantic Oscillation. Hydrol Earth Syst Sci 13:17–25. https://doi.org/10.5194/hess-13-17-2009

Benavides R, Montes F, Rubio A, Osoro K (2007) Geostatistical modelling of air temperature in a mountainous region of Northern Spain. Agric For Meteorol 146:173–188. https://doi.org/10.1016/j.agrformet.2007.05.014

Beniston M (2006) Mountain Weather and Climate: A General Overview and a Focus on Climatic Change in the Alps. Hydrobiologia 562:3–16. https://doi.org/10.1007/s10750-005-1802-0

Bernhardt M, Schulz K (2010) SnowSlide: a simple routine for calculating gravitational snow transport. Geophys Res Lett 37:2010GL043086. https://doi.org/10.1029/2010GL043086

Bickel VT, Manconi A (2022) Decadal surface changes and displacements in Switzerland. J Geovisualization Spat Anal 6(2):24. https://doi.org/10.1007/s41651-022-00119-9

Blöschl G, Kirnbauer R, Gutknecht D (1991) Distributed Snowmelt Simulations in an Alpine Catchment: 1. Model Evaluation on the Basis of Snow Cover Patterns. Water Resour Res 27:3171–3179. https://doi.org/10.1029/91WR02250

Boeckli L, Brenning A, Gruber S, Noetzli J (2012a) A statistical approach to modelling permafrost distribution in the European Alps or similar mountain ranges. Cryosphere 6:125–140. https://doi.org/10.5194/tc-6-125-2012

Boeckli L, Brenning A, Gruber S, Noetzli J (2012b) Permafrost distribution in the European Alps: calculation and evaluation of an index map and summary statistics. Cryosphere 6:807–820. https://doi.org/10.5194/tc-6-807-2012

Braca G, Bussettini M, Gafà RM et al (2022) The Nationwide Water Budget Estimation in the light of the New Permeability Map of Italy. AS-ITJGW 11:31–39. https://doi.org/10.7343/as-2022-575

Cannone N, Diolaiuti G, Guglielmin M, Smiraglia C (2008) Accelerating climate change impacts on alpine glacier forefield ecosystems in the european alps. Ecol Appl 18:637–648. https://doi.org/10.1890/07-1188.1

Cannone N, Gerdol R (2003a) Vegetation as an ecological indicator of surface instability in rock glaciers. Arctic Antarct Alp Res 35:384–390. https://doi.org/10.1657/1523-0430(2003)035%5B0384:VAAEIO%5D2.0.CO;2

Cannone N, Guglielmin M, Hauck C, Mühll DV (2003b) The impact of recent glacier fluctuation and human activities on permafrost distribution, Stelvio Pass (Italian Central-Eastern Alps)

Cannone N, Sgorbati S, Guglielmin M (2007) Unexpected impacts of climate change on alpine vegetation. Front Ecol Environ 5:360–364. https://doi.org/10.1890/1540-9295(2007)5%5B360:UIOCCO%5D2.0.CO;2

Chai T, Draxler RR (2014) Root mean square error (RMSE) or mean absolute error (MAE)? – Arguments against avoiding RMSE in the literature. Geosci Model Dev 7:1247–1250. https://doi.org/10.5194/gmd-7-1247-2014

Chaturvedi V, Ponti S, Guglielmin M (2026) Active layer modelling at Stelvio Pass, Italian Alps. Cold Reg Sci Technol 242:104762. https://doi.org/10.1016/j.coldregions.2025.104762

Chicco D, Warrens MJ, Jurman G (2021) The coefficient of determination R-squared is more informative than SMAPE, MAE, MAPE, MSE and RMSE in regression analysis evaluation. PeerJ Comput Sci 7:e623. https://doi.org/10.7717/peerj-cs.623

Chuanyan Z, Zhongren N, Guodong C (2005) Methods for modelling of temporal and spatial distribution of air temperature at landscape scale in the southern Qilian mountains, China. Ecol Model 189:209–220. https://doi.org/10.1016/j.ecolmodel.2005.03.016

Cohen J, Screen JA, Furtado JC et al (2014) Recent Arctic amplification and extreme mid-latitude weather. Nat Geosci 7:627–637. https://doi.org/10.1038/ngeo2234

Colucci RR, Guglielmin M (2015) Precipitation–temperature changes and evolution of a small glacier in the southeastern European Alps during the last 90 years. Int J Climatol 35:2783–2797. https://doi.org/10.1002/joc.4172

Cortez D, Padilla R, Herrera S et al (2020) Topoclimatic zoning and representative areas as determined by an automatic weather station (AWS) network in the Atacama region, Chile. Atmosphere Basel 11:611. https://doi.org/10.3390/atmos11060611

Duvillard P-A, Ravanel L, Marcer M, Schoeneich P (2019) Recent evolution of damage to infrastructure on permafrost in the French Alps. Reg Envriron Chang 19:1281–1293. https://doi.org/10.1007/s10113-019-01465-z

Duvillard P-A, Ravanel L, Schoeneich P et al (2021) Qualitative risk assessment and strategies for infrastructure on permafrost in the French Alps. Cold Reg Sci Technol 189:103311. https://doi.org/10.1016/j.coldregions.2021.103311

Etzelmüller B, Guglielmin M, Hauck C et al (2020) Twenty years of European mountain permafrost dynamics—the PACE legacy. Environ Res Lett 15:104070. https://doi.org/10.1088/1748-9326/abae9d

Fiddes J, Endrizzi S, Gruber S (2015) Large-area land surface simulations in heterogeneous terrain driven by global data sets: application to mountain permafrost. Cryosphere 9:411–426. https://doi.org/10.5194/tc-9-411-2015

French HM (2017) The periglacial environment. John Wiley & Sons

Frey S, Holzmann H (2015) A conceptual, distributed snow redistribution model. Hydrol Earth Syst Sci 19:4517–4530. https://doi.org/10.5194/hess-19-4517-2015

Gisnås K, Etzelmüller B, Farbrot H et al (2013) CryoGRID 1.0: permafrost distribution in Norway estimated by a spatial numerical model. Permafrost & Periglacial 24:2–19. https://doi.org/10.1002/ppp.1765

Gisnås K, Westermann S, Schuler TV et al (2016) Small-scale variation of snow in a regional permafrost model. Cryosphere 10:1201–1215. https://doi.org/10.5194/tc-10-1201-2016

Gobiet A, Kotlarski S, Beniston M et al (2014) 21st century climate change in the European Alps—a review. Sci Total Environ 493:1138–1151. https://doi.org/10.1016/j.scitotenv.2013.07.050

Grünewald T, Bühler Y, Lehning M (2014) Elevation dependency of mountain snow depth. Cryosphere 8:2381–2394. https://doi.org/10.5194/tc-8-2381-2014

Gruber S (2005) Mountain permafrost: transient spatial modelling, model verification and the use of remote sensing. University of Zurich

Gruber S (2007) A mass-conserving fast algorithm to parameterize gravitational transport and deposition using digital elevation models. Water Resour Res 43:2006WR004868. https://doi.org/10.1029/2006WR004868

Guglielmin M (2004) Observations on permafrost ground thermal regimes from Antarctica and the Italian Alps, and their relevance to global climate change. Glob Planet Change 40:159–167. https://doi.org/10.1016/S0921-8181(03)00106-1

Guglielmin M, Aldighieri B, Testa B (2003) PERMACLIM: a model for the distribution of mountain permafrost, based on climatic observations. Geomorphology 51:245–257. https://doi.org/10.1016/S0169-555X(02)00221-0

Guglielmin M, Bonasera M, Fubelli G et al (2022) Permafrost-based geomorphology of the Mt. Foscagno - Mt. Forcellina ridge (Adda – Inn River basins, Central Italian Alps). J Maps 18:441–447. https://doi.org/10.1080/17445647.2022.2082331

Guglielmin M, Boschi D, D'Agata C, Ellis Evans C, Worland MR (2008) Periglacial and permafrost map of Signy island, South Orkneys Islands, Maritime Antartica. In Proceedings of 9th International Conference on Permafrost (Vol. 1, pp. 569–574). University of Alaska, Inst. of Northern Engineering

Guglielmin M, Camusso M, Polesello S, Valsecchi S (2004) An Old Relict Glacier Body Preserved in Permafrost Environment: The Foscagno Rock Glacier Ice Core (Upper Valtellina, Italian Central Alps). Arct Antarct Alp Res 36:108–116. https://doi.org/10.1657/1523-0430(2004)036%5B0108:AORGBP%5D2.0.CO;2

Guglielmin M, Cannone N, Dramis F (2001) Permafrost–glacial evolution during the Holocene in the Italian Central Alps. Permafr Periglac 12:111–124. https://doi.org/10.1002/ppp.379

Guglielmin M, Donatelli M, Semplice M, Serra Capizzano S (2018) Ground surface temperature reconstruction for the last 500 years obtained from permafrost temperatures observed in the SHARE STELVIO Borehole, Italian Alps. Clim Past 14:709–724. https://doi.org/10.5194/cp-14-709-2018

Guglielmin M, Ponti S, Forte E, Cannone N (2021) Recent thermokarst evolution in the Italian Central Alps. Permafr Periglac 32:299–317. https://doi.org/10.1002/ppp.2099

Guglielmin M, Siletto GB (2000) Carta della Criosfera. Regione Lombardia, Direzione Generale Territorio ed Edilizia Residenziale

Haeberli W, Beniston M (1998) Climate change and its impacts on glaciers and permafrost in the alps

Harris C, Mühll DV, Isaksen K et al (2003) Warming permafrost in European mountains. Glob Planet Change 39:215–225. https://doi.org/10.1016/j.gloplacha.2003.04.001

Henry K, Smith M (2001) A model-based map of ground temperatures for the permafrost regions of Canada. Permafr Periglac 12:389–398. https://doi.org/10.1002/ppp.399

Hjort J, Streletskiy D, Doré G, Wu Q, Bjella K, Luoto M (2022) Impacts of permafrost degradation on infrastructure. Nat Reviews Earth Environ 3:24–38

Hock R (1999) A distributed temperature-index ice- and snowmelt model including potential direct solar radiation. J Glaciol 45:101–111. https://doi.org/10.3189/S0022143000003087

Hock R (2003) Temperature index melt modelling in mountain areas. J Hydrol 282:104–115. https://doi.org/10.1016/S0022-1694(03)00257-9

Hodson TO (2022) Root-mean-square error (RMSE) or mean absolute error (MAE): when to use them or not. Geosci Model Dev 15:5481–5487. https://doi.org/10.5194/gmd-15-5481-2022

Hoelzle M (1992) Permafrost occurrence from BTS measurements and climatic parameters in the eastern Swiss Alps. Permafr Periglac 3:143–147. https://doi.org/10.1002/ppp.3430030212

Ikeda A (2006) Combination of conventional geophysical methods for sounding the composition of rock glaciers in the Swiss Alps. Permafr Periglac 17:35–48. https://doi.org/10.1002/ppp.550

Jonas T, Marty C, Magnusson J (2009) Estimating the snow water equivalent from snow depth measurements in the Swiss Alps. J Hydrol 378:161–167. https://doi.org/10.1016/j.jhydrol.2009.09.021

Keller F (1992) Automated mapping of mountain permafrost using the program PERMAKART within the geographical information system ARC/INFO. Permafr Periglac 3:133–138. https://doi.org/10.1002/ppp.3430030210

Lehning M, Bartelt P, Brown B et al (1999) snowpack model calculations for avalanche warning based upon a new network of weather and snow stations. Cold Reg Sci Technol 30:145–157. https://doi.org/10.1016/S0165-232X(99)00022-1

Lehning M, Völksch I, Gustafsson D et al (2006) ALPINE3D: a detailed model of mountain surface processes and its application to snow hydrology. Hydrol Process 20:2111–2128. https://doi.org/10.1002/hyp.6204

Liston GE, Sturm M (1998) A snow-transport model for complex terrain. J Glaciol 44:498–516. https://doi.org/10.3189/S0022143000002021

Luijting H, Vikhamar-Schuler D, Aspelien T et al (2018) Forcing the SURFEX/Crocus snow model with combined hourly meteorological forecasts and gridded observations in southern Norway. Cryosphere 12:2123–2145. https://doi.org/10.5194/tc-12-2123-2018

Magnusson J, Farinotti D, Jonas T, Bavay M (2011) Quantitative evaluation of different hydrological modelling approaches in a partly glacierized Swiss watershed. Hydrol Process 25:2071–2084. https://doi.org/10.1002/hyp.7958

Malfasi F, Cannone N (2021) Phytosociology of the vegetation communities of the Stelvio Pass area. J Maps 17:367–375. https://doi.org/10.1080/17445647.2021.1957033

Montrasio A, Berra F, Cariboni M, Ceriani M, Deichmann N, Ferliga C, Gregnanin A,Guerra S, Gugliemin M, Jadoul F, Longhin M (2012) CARG - Carta geologica nazionale scala 1:50.000 - Note illustrative del Foglio geologico 024BORMIO, p. 120

Mott R, Vionnet V, Grünewald T (2018) The seasonal snow cover dynamics: review on wind-driven coupling processes. Front Earth Sci 6:197. https://doi.org/10.3389/feart.2018.00197

Muller SW (1945) Permafrost or permanently frozen ground and related engineering problems. Army map service, US Army

Noetzli J, Isaksen K, Barnett J et al (2025) Enhanced warming of European mountain permafrost in the early 21st century. Nat Commun 15:10508. https://doi.org/10.1038/s41467-024-54831-9

Obu J, Westermann S, Bartsch A et al (2019) Northern Hemisphere permafrost map based on TTOP modelling for 2000–2016 at 1 km2 scale. Earth Sci Rev 193:299–316. https://doi.org/10.1016/j.earscirev.2019.04.023

Oliva M, Žebre M, Guglielmin M et al (2018) Permafrost conditions in the Mediterranean region since the Last Glaciation. Earth Sci Rev 185:397–436. https://doi.org/10.1016/j.earscirev.2018.06.018

Orsolini Y, Wegmann M, Dutra E et al (2019) Evaluation of snow depth and snow cover over the Tibetan Plateau in global reanalyses using in situ and satellite remote sensing observations. Cryosphere 13:2221–2239. https://doi.org/10.5194/tc-13-2221-2019

Ou C, LaRocque A, Leblon B et al (2016) Modelling and mapping permafrost at high spatial resolution using Landsat and Radarsat-2 images in Northern Ontario, Canada: Part 2 – regional mapping. Int J Remote Sens 37:2751–2779. https://doi.org/10.1080/01431161.2016.1151574

Pavan V, Antolini G, Barbiero R et al (2019) High resolution climate precipitation analysis for north-central Italy, 1961–2015. Clim Dyn 52:3435–3453. https://doi.org/10.1007/s00382-018-4337-6

Pavoni M, Guglielmin M, Bast A, Ponti S, Forte E, Carrera A et al (2026) Brief communication: on the potential of dual-coil frequency-domain electromagnetic (FDEM) systems to detect frozen layers in mountain permafrost environments. EGUsphere, 2026, 1–8. https://doi.org/10.5194/egusphere-2026-1264

Pepin NC, Arnone E, Gobiet A et al (2022) Climate changes and their elevational patterns in the mountains of the world. Rev Geophys 60:e2020RG000730. https://doi.org/10.1029/2020RG000730

Pomeroy JW, Gray DM (1990) Saltation of snow. Water Resour Res 26:1583–1594. https://doi.org/10.1029/WR026i007p01583

Ponti S, Cannone N, Guglielmin M (2020) A new simple topo-climatic model to predict surface displacement in paraglacial and periglacial mountains of the European Alps: The importance of ground heating index and floristic components as ecological indicators. Ecol Ind 120:106889. https://doi.org/10.1016/j.ecolind.2020.106889

Ponti S, Girola I, Guglielmin M (2024) Thermal photogrammetry on a permafrost rock wall for the active layer monitoring. Sci Total Environ 917:170391. https://doi.org/10.1016/j.scitotenv.2024.170391

Regione Lombardia (2016) Ghiacciai della Lombardia. Geoportale della Lombardia

Richter B, Schweizer J, Rotach MW, Van Herwijnen A (2019) Validating modeled critical crack length for crack propagation in the snow cover model SNOWPACK. Cryosphere 13:3353–3366. https://doi.org/10.5194/tc-13-3353-2019

Roe GH, Baker MB (2006) Microphysical and Geometrical Controls on the Pattern of Orographic Precipitation. J Atmos Sci 63:861–880. https://doi.org/10.1175/JAS3619.1

Rolland C (2003) Spatial and seasonal variations of air temperature lapse rates in Alpine regions. J Clim 16:1032–1046

Sannino C, Borruso L, Mezzasoma A et al (2021) Abiotic factors affecting the bacterial and fungal diversity of permafrost in a rock glacier in the Stelvio Pass (Italian Central Alps). Appl Soil Ecol 166:104079. https://doi.org/10.1016/j.apsoil.2021.104079

Santi E, Pettinato S, Paloscia S et al (2014) Monitoring of Alpine snow using satellite radiometers and artificial neural networks. Remote Sens Environ 144:179–186. https://doi.org/10.1016/j.rse.2014.01.012

Serreze MC, Barry RG (2011) Processes and impacts of Arctic amplification: A research synthesis. Glob Planet Change 77:85–96. https://doi.org/10.1016/j.gloplacha.2011.03.004

Smith MW, Riseborough DW (1996) Permafrost monitoring and detection of climate change. Permafr Periglac 7:301–309

Smith MW, Riseborough DW (2002) Climate and the limits of permafrost: a zonal analysis. Permafr Periglac 13:1–15. https://doi.org/10.1002/ppp.410

Soncini A, Bocchiola D, Confortola G et al (2016) Future hydrological regimes and glacier cover in the Everest region: The case study of the upper Dudh Koshi basin. Sci Total Environ 565:1084–1101. https://doi.org/10.1016/j.scitotenv.2016.05.138

Sovilla B, McElwaine JN, Schaer M, Vallet J (2010) Variation of deposition depth with slope angle in snow avalanches: Measurements from Vallée de la Sionne. J Geophys Res 115:2009JF001390. https://doi.org/10.1029/2009JF001390

Stenni B, Genoni L, Flora O, Guglielmin M (2007) An oxygen isotope record from the Foscagno rock-glacier ice core, Upper Valtellina, Italian Central Alps. Holocene 17:1033–1039. https://doi.org/10.1177/0959683607082438

Stocker-Mittaz C, Hoelzle M, Haeberli W (2002) Modelling alpine permafrost distribution based on energy-balance data: a first step. Permafr Periglac 13:271–282. https://doi.org/10.1002/ppp.426

Sturm M, Holmgren J, König M, Morris K (1997) The thermal conductivity of seasonal snow. J Glaciol 43:26–41. https://doi.org/10.3189/S0022143000002781

Tarquini S, Isola I, Favalli M, Battistin A, Dotta GT (2023) a Digital Elevation Model of Italy with a 10 Meters Cell Size (Version 1.1), vol 1. Istituto Nazionale di Geofisica e Vulcanologia (INGV), Roma, Italy, pp 1–2

Taylor JR (2022) An introduction to error analysis: the study of uncertainties in physical measurements. MIT Press

Vionnet V, Six D, Auger L et al (2019) Sub-kilometer precipitation datasets for snowpack and glacier modeling in Alpine terrain. Front Earth Sci 7:182. https://doi.org/10.3389/feart.2019.00182

Wang C, Guo D, Zang S (2023) Thermal remote sensing for mapping the sub-Arctic permafrost and refining its southern limits. Int J Appl Earth Obs Geoinf 118:103235. https://doi.org/10.1016/j.jag.2023.103235

Westermann S, Ingeman-Nielsen T, Scheer J et al (2023) The CryoGrid community model (version 1.0) – a multi-physics toolbox for climate-driven simulations in the terrestrial cryosphere. Geosci Model Dev 16:2607–2647. https://doi.org/10.5194/gmd-16-2607-2023

Westermann S, Langer M, Boike J et al (2016) Simulating the thermal regime and thaw processes of ice-rich permafrost ground with the land-surface model CryoGrid 3. Geosci Model Dev 9:523–546. https://doi.org/10.5194/gmd-9-523-2016

Westermann S, Schuler TV, Gisnås K, Etzelmüller B (2013) Transient thermal modeling of permafrost conditions in Southern Norway. Cryosphere 7:719–739. https://doi.org/10.5194/tc-7-719-2013

Willmott C, Matsuura K (2005) Advantages of the mean absolute error (MAE) over the root mean square error (RMSE) in assessing average model performance. Clim Res 30:79–82. https://doi.org/10.3354/cr030079

Zhong X-Y, Zhang T, Su H et al (2021) Impacts of landscape and climatic factors on snow cover in the Altai Mountains, China. Adv Clim Change Res 12:95–107. https://doi.org/10.1016/j.accre.2021.01.005